

Red wine gold nanoparticles for wound healing



UNIVERSITY *of the*
WESTERN CAPE

Tswellang Mgijima (BSc Hons, Chemistry)

Supervisor: Prof MO Onani

Co-supervisor: Dr NRS Sibuyi

Red wine gold nanoparticles for wound healing

ABSTRACT

Gold nanoparticles (AuNPs) have unique properties giving them a wide range of applications in various fields including the biomedical fields. Their synthesis through chemical and physical methods has been explored and demonstrated to be toxic and harmful to the environment. The introduction of biogenic synthesis offers a more effective, less toxic, and cost-effective alternative route for the synthesis of AuNPs. In the biogenic synthesis, phytochemicals present in plants or biomolecules from microorganisms are used as reducing and stabilizing agents in the reduction of gold precursor to AuNPs. Plants and their products such as red wines in our case are preferred over microorganisms as they are readily available, inexpensive, and can synthesize AuNPs in a single step. The AuNPs have shown great potential in wound healing, by demonstrating anti-inflammatory, antioxidant, and antibacterial activities. These properties present a therapeutic window for wound healing for the red wine-derived nanoparticles. The biosynthesis and wound healing effect of AuNPs synthesized from three different red wine extracts (RW-Es) were investigated in this study.

Three RWs: *Pinot noir* (PN), *Pinotage* (P), *Cabernet Sauvignon* (CS); were purchased from Checkers Liquor store in Cape Town, South Africa. The wine solvents were dried by the use of a rotary evaporator and the product dried at 70°C in an oven overnight. Stock solutions of 25mg/mL PN, 12,5mg/mL CS and 50mg/mL P were prepared in deionized water (dH₂O) and mixed with 1mM gold salt (HAuCl₄) to synthesize PN-AuNPs, CS-AuNPs, and P-AuNPs, respectively. The synthesis process of all the RW-AuNPs was carried out with help of a thermo-mixer which was operated at 1000rpm while optimizing various reaction parameters such as temperature, pH, RW-E concentration, and the concentration of gold salt. The AuNP synthesis was monitored by colour changes and was later characterized by Ultraviolet-visible spectroscopy (UV-Vis), dynamic light scattering, and the Fourier Transform Infrared Spectroscopy (FT-IR).

The concentration of the resulting AuNPs was evaluated by Inductively Coupled Plasma Atomic Optical Emission Spectroscopy (ICP-OES). The stability of the AuNPs in various solutions (Water, FBS, PBS, and DMEM) was evaluated by monitoring changes in the UV-Vis spectra of the solutions after incubation at 37°C throughout 24hrs. The antioxidant activity of the RW-Es and the RW-AuNPs was evaluated by the DPPH assay. The effect of the RW-Es

and RW-AuNPs was evaluated by MTT assay after exposure to KMST-6 cells for 24-72 hrs. The application of RW-AuNPs in wound healing was investigated by the scratch assay on KMST-6 cells.

The study demonstrated the feasibility of PN, CS, and P extracts in the synthesis of RW-AuNPs. The presence of RW-AuNPs in the solution was confirmed by UV-Vis with an absorption peak of around 550nm. The hydrodynamic sizes of the RW-AuNPs ranged between 10 -100 nm. FT-IR spectra showed a chemical shift around 3300cm^{-1} confirming the involvement of polyphenols in the reduction of Au ions. There were also some noticeable shifts in spectra of the RW-Es compared to the RW-AuNPs suggesting that other functional groups present in esters, carboxylic acids, and amino acids could also have played a role in the reduction of Au ions. Based on the DPPH assay, the RW-Es had higher antioxidant activity than their corresponding AuNPs. There were no apparent or significant changes in the peak positions and maximum absorbance of the RW-AuNPs after incubation in different solutions for 24 hrs, suggesting that the AuNPs were stable in these solutions. The RW-Es and RW-AuNPs were non-toxic to the KMST-6 cells up to 72 hrs and the cells showed enhanced cell viability when treated with the RW-AuNPs. The results presented in this study indicated the potential use of biogenic RW-AuNPs in wound healing giving this study one of a first of its kind to the best of our knowledge.



UNIVERSITY of the
WESTERN CAPE

KEYWORDS

Antioxidant Activity

Cabernet Sauvignon Red Wine

Gold Nanoparticles

Green Synthesis

Nanotechnology

Pinot Noir Red Wine

Pinotage Red Wine

Red Wine

Wound Healing

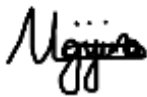


DECLARATION

I, Tswellang Mgijima declare that this study titled “Red wine gold nanoparticles for wound healing” is my own work and has not been submitted before any degree or examination at this university or other tertiary institution. All the sources I have used or quoted have been indicated and duly acknowledged by complete referencing.



Signature

A handwritten signature in black ink, appearing to read "Mgijima".

Date 09/03/2022

ACKNOWLEDGEMENTS

First and foremost, praises and thanks to God the Almighty for remaining a pillar of strength throughout this project.

A special thanks to my parents: **Henry** and **Vuyiswa Mgijima**; my siblings: **Mfundokazi, Lindiwe, Reabetsoe** and **Reaboka Mgijima** for the support, and thank you for being my motivation.

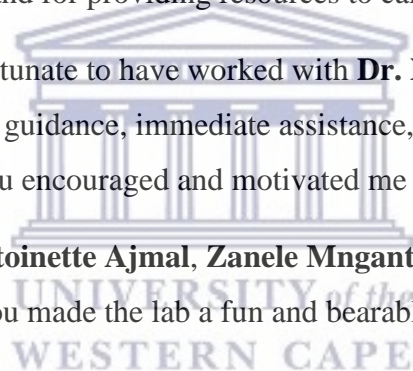
I wish to also express my sincere gratitude to **Prof. M Onani**, professor of Inorganic Chemistry for giving me the opportunity to do my research because this work would not have been possible without his guidance and support.

I would like to show my appreciation to **Prof. Mervin Meyer** and **Prof. Abram Madiehe** for allowing me to use the lab and for providing resources to carry out my research.

I consider myself to be very fortunate to have worked with **Dr. Nicole Sibuyi**, my co-supervisor. Thank you for your guidance, immediate assistance, and motivation. Numerous times my will failed me, but you encouraged and motivated me to continue.

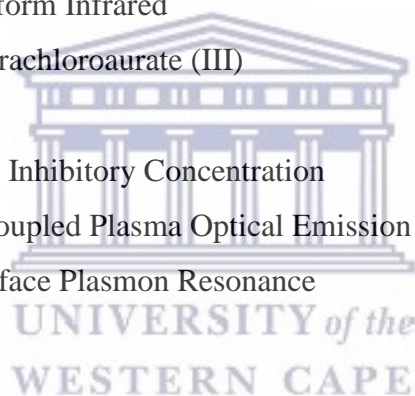
I also express my thanks to **Antoinette Ajmal, Zanele Mnganto-Khuselo** and **Sohail Simon** for a dependable friendship. You made the lab a fun and bearable environment.

I would also like to thank the **DSI National Nanoscience Post Graduate Teaching and Training Platform** and **Mrs. Valencia Jamalie** for the opportunity to follow my dreams.



LIST OF ABBREVIATIONS

°C	Degrees Celsius
AuNPs	Gold Nanoparticles
CS	Cabernet Sauvignon
dH ₂ O	Deionized Water
DMEM	Dulbeccos Modified Eagles' Medium
DMSO	Dimethyl Sulphoxide
E	Extract
Est	Established
EMU	Electron Microscope Unit
FBS	Fetal Bovine Serum
FTIR	Fourier Transform Infrared
HAuCl ₄	Hydrogen Tetrachloroaurate (III)
Hr	Hour
IC ₅₀	Half Maximal Inhibitory Concentration
ICP-OES	Inductively Coupled Plasma Optical Emission Spectroscopy
LSPR	Localized Surface Plasmon Resonance
M	Molar
mg	Milligram
min	Minute
mL	Millilitre
mm	Millimeter
mM	Millimolar
MNPs	Metal Nanoparticles
MTT	3-[4,5-Dimethylthiazol-2-Yl]-2,5-Diphenyltetrazolium Bromide
NaBH ₄	Sodium Borohydride
NPs	Nanoparticles
P	Pinotage
PBS	Phosphate Buffered Saline
PN	Pinot Noir
ROS	Reactive Oxygen Species
RW	Red Wine



RW-AuNPs	Red Wine Gold Nanoparticles
RWE	Red Wine Extract
SEM	Scanning Electron Microscope
SPR	Surface Plasmon Resonance
t	Time
TEM	Transmission Electron Microscope
TNF- α	Tumour necrosis factor- α
UCT	University of Cape Town
UV-VIS	Ultraviolet Visible
λ_{\max}	Maximum Absorbance
%	Percentage
~	Approximate



LIST OF FIGURES

Figure 1.1 The four main wound healing stages, hemostasis, inflammatory, proliferation and remodeling with modifications

Figure 1.2 The bottom up (a) and top down (b) approaches for synthesis of NPs

Figure 1.3 Mechanism for the synthesis of NPs using plant extracts as reducing and stabilizing agents.

Figure 3.1 PN-AuNPs synthesized from different concentrations of PN-E and 1mM gold salt at 25°C.

Figure 3.2 UV-Vis spectra of RW-AuNPs synthesized at temperatures 25°C, 50°C, 70°C and 99°C on a thermo-shaker operating at 1000rpm for 1hr for varying PN- and P-E concentrations

Figure 3.3 The effect of gold salt concentrations is the synthesis of RW-AuNPs. 0,25, 0,5, 0,75, 1, 2, 3, 4 and 5mM H₂AuCl₄ are used in the synthesis performed on a thermo-shaker operating at 1000rpm at optimized temperatures.

Figure 3.4 Effect of increasing RWE pH on the RW-AuNP synthesis

Figure 3.5 UV-Vis spectra of SPR bands representing AuNPs formed from (a) CS, (b) P and (PN) extracts at extract pH, pH 4, 5, 6, 7, 8, 9 and 10 using optimized concentrations and temperature.

Figure 3.6 UV-Vis spectra recorded as a function of time for the synthesis of AuNPs using (a) CSRW, (b) PRW, and (c) PNRW extracts at optimized pH, temperature, and concentration of extracts. (d), (e) and (f) is the change in absorbance maxima recorded with time.

Figure 3.7 The overall synthesis of AuNPs from RW extracts.

Figure 3.8 Schematic representation of UV-Vis of PN-AuNPs, CS-AuNPs, and P-AuNPs synthesized at optimal reaction parameters.

Figure 3.9 The hydrodynamic size distribution of CS (a), P (b), and PN (c) AuNPs synthesized at the optimal conditions.

Figure 3.10 FT-IR spectra of RWE and the resulting AuNPs.

Figure 4.1 Investigation of the antioxidant activity of RW extracts and AuNPs in relation to ascorbic acid using DPPH assay. a) % Inhibition for RW-E, b) RW-AuNPs and c) AA used as a standard.

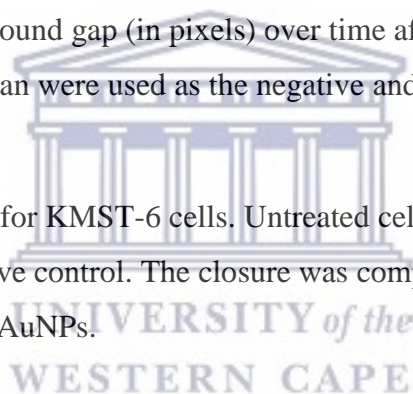
Figure 4.2 *In vitro* stability of RW-AuNPs during incubation at 37°C in solution. UV-Vis spectra were taken periodically for 24hrs.

Figure 4.3 Effect of RW-Es and RW-AuNPs on KMST-6 cells. The cells were treated with increasing concentrations of RW-Es (a) ranging between 0.005 - 1mg/mL and RW-AuNPs (b) at 1.5625 - 50µg/mL for 24hr and cell viability was measured by MTT assay.

Figure 4.4 Effect of RW-AuNPs on KMST cell migration using a scratch assay. Scratch images were taken at 0h, 24h, 48h and 72h after treatment with CS-AuNPs, PN-AuNPs and P-AuNPs and Allantoin as a positive control

Figure 4.5 Change in area of wound gap (in pixels) over time after treatment with CS, PN, P AuNPs. Untreated cells and Allantoin were used as the negative and positive controls respectively.

Figure 4.6 Wound closure (%) for KMST-6 cells. Untreated cells were used as a negative control and allantoin as a positive control. The closure was compared to cells treated with CS-AuNPs, PN-AuNPs, and P-AuNPs.



LIST OF TABLES

Table 1.1 Current technologies for wound healing

Table 1.2 Application of AuNPs

Table 2.1 List of chemicals

Table 2.2 List of instruments

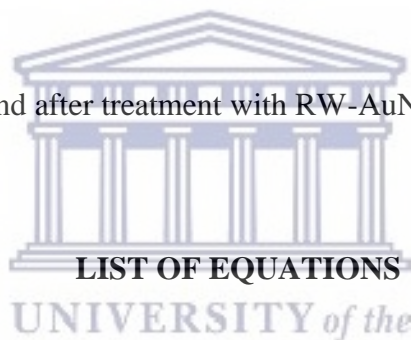
Table 2.3 Cell line

Table 3.1 Optimal conditions for reaction parameters for AuNPs synthesis.

Table 3.2 Summary of the optical and DLS properties of the RW-AuNPs.

Table 3.3 Major peak shifts and their positions in the RW extracts as compared to their RW AuNPs.

Table 4.1 Cell density before and after treatment with RW-AuNPs



EQ 2.1 % Inhibition = $\frac{A_{control} - A_{test}}{A_{control}} \times 100$

EQ 2.2 % Cell viability = $\left(\frac{\text{mean untreated}}{\text{mean treated}}\right) \times 100$

EQ 2.3 % Wound closure = $\frac{(\text{pre-migration}) - (\text{migration})}{\text{pre-migration}} \times 100$

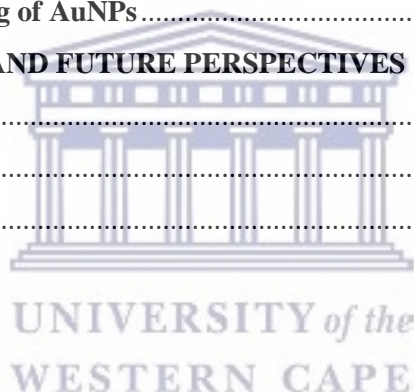
EQ 3.1 Rate of reaction = $\frac{\Delta OD \text{ at } \lambda_{max}}{\Delta \text{time}(\text{min})}$

EQ 4.1 % Increase in number of cells = $\frac{\text{number of cells at } t_{72} - \text{number of cells at } t_0}{\text{number of cells at } t_0} \times 100$

TABLE OF CONTENTS

ABSTRACT.....	i
KEYWORDS.....	iii
DECLARATION.....	iv
ACKNOWLEDGEMENTS	v
LIST OF ABBREVIATIONS	vi
LIST OF FIGURES	viii
LIST OF TABLES	x
LIST OF EQUATIONS.....	x
TABLE OF CONTENTS	xi
Thesis overview	1
Problem statement	1
CHAPTER 1: LITERATURE REVIEW.....	3
1.1 Introduction.....	3
1.2 The application of green synthesized nanoparticles in wound healing.....	4
1.2.1 Wound Healing.....	4
1.2.2 AuNPs.....	8
1.2.3. Methods of AuNP synthesis.....	9
1.2.4 Applications of AuNPs.....	14
1.2.5 Wound healing effect of RW-AuNPs.....	17
1.3 Objectives.....	21
CHAPTER 2: MATERIALS AND METHODS	22
2.1 Materials	22
2.2 Methodology	23
2.2.1 Preparation of RW extracts (RW-Es)	23
2.2.2 Synthesis and characterization of RW-AuNPs.....	24
2.2.3 Reaction Kinetics.....	25
2.3 Characterization of the AuNPs.....	25
2.3.1 UV-Vis Analysis	25
2.3.2 DLS analysis	25
2.3.3 FT-IR Spectroscopy analysis.....	25
2.3.4 <i>In vitro</i> stability test.....	26
2.3.5 Quantification of RW-AuNPs by ICP-OES.....	26
2.3.6 Antioxidant Activity of RW-Es and AuNPs: DPPH assay	26

2.4 Effect of RW extracts and AuNPs on cell viability	27
2.5. Scratch Assay	28
CHAPTER 3: RESULTS AND DISCUSSION	30
3.1 Synthesis and characterization of RW-AuNPs.....	30
3.1.1 Optimization of RW-AuNPs synthesis.....	30
3.1.2 Reaction Kinetics for synthesis of RW-AuNPs.....	37
3.1.3 Biosynthesis of RW-AuNPs using optimal conditions	40
3.1.4 Optical properties of RW-AuNPs.....	41
3.1.5 DLS analysis	42
3.1.6 FT-IR analysis	45
3.2 Biological Assay.....	50
3.2.1 Determination of RW-AuNPs concentrations	50
3.2.2 <i>In vitro</i> antioxidant activity	50
3.2.3 <i>In vitro</i> stability testing of AuNPs.....	52
CHAPTER 4: CONCLUSION AND FUTURE PERSPECTIVES	61
4.1 Conclusion	61
4.2 Recommendations.....	61
REFERENCES.....	63



Thesis overview

The current study reports on the preparation of red wine extracts (RW-Es), the synthesis of AuNPs through green chemistry, and the characterization of the resulting RW-AuNPs. Three RWs: CS, PN and P were used as reducing and stabilizing agents in the synthesis of RW-AuNPs. The concentration of AuNPs was determined by ICP-OES and the stability of these AuNPs in cell culture media was evaluated. The cell viability of human skin fibroblast (KMST-6) cells treated with the RW-AuNPs was tested using the MTT assay. The wound healing potential of the RW-AuNPs was evaluated *in vitro* by scratch assay on KMST cells. The thesis is composed of four chapters as outlined below:

Chapter 1: Literature review which gives a presentation of the background of the study, including nanotechnology and AuNPs and their applications. The literature on the different methods of AuNPs synthesis and application in wound healing is reviewed. The aims and objectives of the study are also discussed.

Chapter 2: Describes the materials and methods used in the synthesis and characterization RW-AuNPs; as well as their biological activities.

Chapter 3: Describes and discusses the results obtained from the synthesis and characterization RW-AuNPs; as well as their biological activities.

Chapter 4: Conclusion and future perspectives, summarizes the findings of the study and gives recommendations for future work.

Problem statement

The burden posed by wounds on patients and the healthcare system is huge. Approximately 8.2 million people are affected by wounds (Nqakala *et al.*, 2021). This is a growing pressure on the health system, and it requires immediate attention. Wounds have a natural way of healing, and wound dressings are often used to protect the wound from infections and enhance their healing. Antibacterial creams and ointments are capable of not only preserving the environment but also transporting therapeutic agents to accelerate wound healing. Repeated and un-administered use of these antibacterial creams often results in antibacterial resistance (Naskar & Kim, 2020).

When the infections develop, a person's health and quality of life are adversely affected. Bacteria can frequently colonize and proliferate in the exposed tissues, and when established,

these bacteria can pass through the blood capillaries of the tissues, which may eventually lead to bacteraemia (Minasyan, 2019). This is a global challenge and a growing health crisis and a lot of money are invested in wound care (Nqakala *et al.*, 2021). Present interventions such as wound dressings and antibiotics are expensive and time-consuming, and not always effective. Novel strategies with sustainable therapeutic effects are sought. Nanotechnology presents innovative means to improve and modify the current technologies and make them suitable and effective for wound healing. An ointment with AuNPs will decrease the bacterial load, and thus prevent wound infections. Nanomaterials can be used for two types of applications in wound healing as drug delivery vehicles or as a treatment to promote wound healing (Naskar & Kim, 2020).

Incorporation of drugs to these NPs allows for a more targeted drug delivery, resolves the poor drug solubility, and increases their efficacy (Mordorski *et al.*, 2015). The NPs increase the likelihood of interaction with their biological target. Nanofibers can also be used for dual functions in wound healing as antibacterial agents and dressings, and this can facilitate collagen synthesis as well as the re-epithelization of wounds (Shahverdi *et al.*, 2014; Wu *et al.*, 2014). One of the innovative nanotechnology strategies is the use of AuNPs in the development of effective wound healing agents, they can be incorporated into existing ointments for synergistic wound healing effects. The main advantage is that the cost can be reduced significantly because these are incorporated into pre-existing technologies rather than re-inventing the wheels. The green synthesis of AuNPs is also cost-effective, abides by the rules of green chemistry, and is time-efficient (Sherwani *et al.*, 2015) and (Hsu *et al.*, 2011).

CHAPTER 1: LITERATURE REVIEW

1.1 Introduction

Nanotechnology plays a huge and highly significant role in medicine, where nanomaterials are used for various applications as diagnostic or therapeutic agents (Baetke *et al.*, 2015). These particles are classified into metal, fullerenes, ceramic and polymeric NPs. The AuNPs are among the MNPs used in biophysical and medical fields due to their size related to optical, electronic, magnetic, catalytic, and biocompatibility properties (Khan *et al.*, 2019).

AuNPs are pure metallic gold structures characterized by at least one 100nm dimension (Rai *et al.*, 2016). The AuNPs can contain oxidized centres which can undergo *in situ* reductions by the substrate (Hashmi *et al.*, 2006) and can therefore be used in important chemical reactions. As a result of this application, there is a large demand for their production on a large scale. Various physical and chemical methods can be used in the synthesis and production of AuNPs. However, these methods tend to be expensive and require the use of toxic materials. The green chemistry route offers a safer and less expensive alternative. Green chemistry is defined as the area of chemistry that designs processes that reduce the use and generation of harmful substances (Saleh & Koller, 2018).

It has recently been discovered that biological materials such as fungi, plants, and bacteria can be used to transform inorganic metal ions into MNPs. The basic principle of the synthesis of AuNPs by biological materials is that the constituents of the extract can act as reductants of ionic gold, which exist in the oxidation state III in chloroauric acid to ground state (Masala & Seshadri, 2004). In the case of microorganisms, the enzymes produced by the organisms are used to reduce the ionic gold (Moghaddam *et al.*, 2015). Plants extracts are receiving more interest in green synthesis as they are readily available and therefore inexpensive. The synthesis of NPs using plants requires less energy input (Ali *et al.*, 2020).

Red wine (RW) is an alcoholic beverage with a chemical composition comprising of ethyl sugars, polyphenols, and organic acids. Resveratrol is one of the polyphenols present in RW that is passed on from grape seeds and skins to the wine during production. This compound possesses anti-inflammatory, antioxidant, and cardioprotective properties (Salehi *et al.*, 2018). This compound is produced by plants to increase their survival and resistance to diseases that result from infections and climate change. When one consumes these plants,

they can acquire similar protection, hence it is known to have health benefits to humans (Koushki *et al.*, 2018). Although this is the case, consuming large amounts of wine is not recommended because alcohol itself is neurotoxic (Markoski *et al.*, 2016). RW-Es, in particular PN, has been used to synthesize AuNPs, however, their wound healing effect has not been reported before and they are investigated in this study.

1.2 The application of green synthesized nanoparticles in wound healing

1.2.1 Wound Healing

The skin is the largest organ in the body and serves to protect the internal organs from external harm. Wounds occur when the skin (external wounds) or the tissues (internal wounds) are subjected to cuts or injuries thereby disrupting their normal anatomy. Wounds are classified as acute or chronic wounds based on the duration they take to heal. The physiological response of the body to injuries is well-coordinated. Wounds that follow the natural response are known as acute wounds, and those whose process is interrupted as chronic or indolent wounds. Acute wounds result from cuts or surgical incisions and often lead to efficient wound healing lasting between 2-3 weeks (Nqakala *et al.*, 2021);(Dreifke *et al.*, 2015). Chronic wounds on the other hand can take three months to years to heal. These wounds result from bacterial infections, diabetes, malnutrition among other factors. The abnormal healing process in chronic wounds is due to the prolonged inflammation stage (Agyare *et al.*, 2016).

Wounds have a natural way of healing. After sustaining an injury, the body enters a survival mode to remove the damaged or destroyed cells and regenerate tissue (Beldon, 2010) . Depending on the depth of the wound, the process of healing takes a minimum of 7 days. The wound healing process is a natural response consisting of four overlapping stages involved in the repair of the damaged skin cells as shown in **Figure 1.1**: the homeostasis, inflammatory, proliferative, and remodelling stages (Elbagory *et al.*, 2016);(Tyavambiza *et al.*, 2021);(Nqakala *et al.*, 2021).

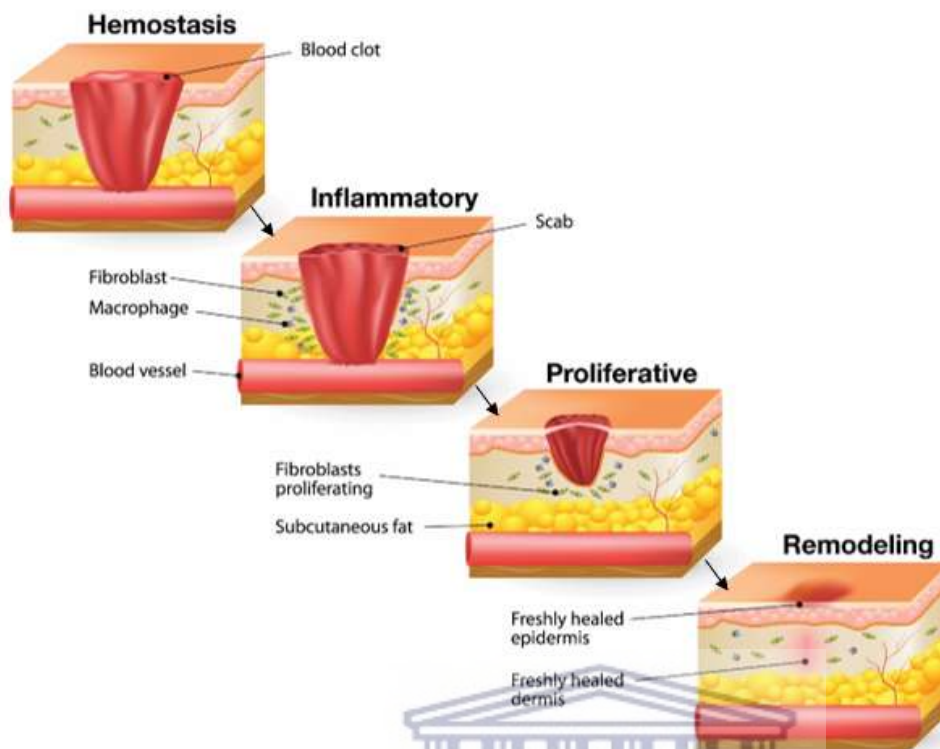


Figure 1.1 The four main wound healing stages, hemostasis, inflammatory, proliferation and remodeling. Reprinted with permission from MDPI (Nqakala *et al.*, 2021) with modifications.

The homeostasis and the inflammatory stages begin right after the injury. The first stage is characterized by the vascular response to ensure homeostasis and blood coagulation (Elbagory *et al.*, 2016);(Nqakala *et al.*, 2021). The homeostasis stage ensures wound closure through blood clotting, whereby the blood vessels begin to constrict immediately after injury to stop blood flow. Then platelets assemble at the injury site with fibrin threads and collagen acting as molecular binding agents. The inflammatory stage precedes the homeostasis stage and is characterized by the removal and destruction of debris and bacteria to prepare for the growth of new tissue in the wound area (Singh *et al.*, 2017). A fluid-like substance or transudate which consists of protein, water, and salt, leaks out of the wound and flushes out the dead cells, pathogens, and bacteria. Then the growth factors, white blood cells, and nutrients accumulate on the wound site and this process causes the swelling at the wound. This is followed by the proliferation stage where granulation of the tissue begins to fill up the wound site which usually takes two weeks. This stage is aimed at filling and closing the wound with collagen and extracellular matrix. It consists of three distinct phases: filling of the wound, construction of wound margins, and epithelization. These phases occur within a period of 24 days after injury. Once the new tissue is formed, the remodeling phase initiates

to restore the structural integrity and function of the newly formed tissue. Collagen is remodeled and the newly formed tissue gains strength and flexibility. Cross-linking of the collagen fibers makes the scar region stronger. The cells that are no longer needed for this process are removed through programmed cell death (apoptosis). Remodeling can take up to two years. However, the healing process can be affected by either external or internal factors such as underlying comorbidities (diabetes), entrapped foreign material, and wound infection. All of these factors might prolong the wound healing process beyond 2 years or prevent the wound from completely healing (Nqakala *et al.*, 2021).

1.2.1.1 Wound healing treatments

Wounds are supposed to heal naturally by following the stages outlined in **Figure 1.1**, and in some instances wound healing agents can be used to accelerate wound healing and prevent wound infections. Various methods have been implemented to ensure optimal wound healing, these include wound swabbing, cleaning, dressing, and debridement (Dreifke *et al.*, 2014). Acute wounds can be regularly cleaned using a salt solution and dressed until it is completely healed; but chronic wounds take a longer period to heal and require constant wound care to remove the inflamed or dead skin (Margolis *et al.*, 2011). The wound dressings protect the wound from the environment. **Table 1.1** shows the convectional technologies implemented in wound healing, how they benefit or accelerate wound healing, and their limitations.

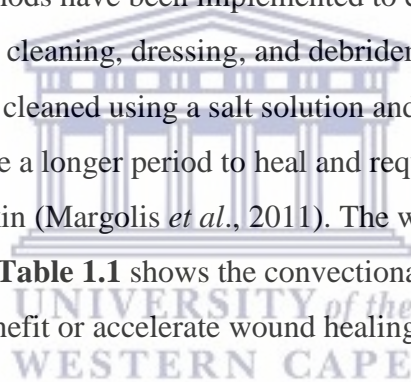


Table 1.1 Current wound healing methods and their limitations

Type of therapy	Benefits	Commercialized products	Limitations	Refs
Traditional gauze dressings	Shield open wounds from bacterial invasion.	Urgotul SSD™	Cotton gauze needs to be removed which causes more damage	(Han 2015; Nqakala <i>et al.</i> , 2021; Murray <i>et al.</i> , 2019)
Cell growth therapy	The regenerative strategy provides similar skin from stem cells minimizing scarring and color mismatch.		May affect and impair natural growth factors, stem cell quantity, and viability.	(Han, 2015) ¹
Anti-bacterial creams and ointments	Preserve the wound environment and accelerate wound healing.		Repeated use of these antibacterial creams often results in antibacterial resistance	(Shahverdi <i>et al.</i> , 2014)
Silver products	Exhibit antibacterial effects and can be used on infected chronic wounds and burns.	KoCarbonAg®	It may be toxic to surrounding tissue	(Mihai <i>et al.</i> , 2019)
Biomaterial based dressing and skin substitutes	Restore the functional components of the skin for the regeneration and the migration of epithelial cells. Collagen, Chitosan, and hyaluronic acid incorporated dressings enhance wound healing by providing such an environment.		Reduce vascularization	(Dhivya <i>et al.</i> , 2015)
Hydrogels	Hydrogels are hydrophilic materials consisting of 70% to 90% water content. These are non-irritant and permeable to metabolites providing a moist environment.	Nu-gel™, Aquaform™	Not effective for infectious wounds. Almost non-adhesive and therefore require a secondary dressing.	(Dhivya <i>et al.</i> , 2015; Han, 2015)

¹ (Murray *et al.*, 2019)(Murray *et al.*, 2019)(Murray *et al.*, 2019)Murray *et al.*, “Development and Use of Biomaterials as Wound Healing Therapies.”

These conventional methods offer satisfactory wound therapy. However their applications are hindered by cost, side effects, and reduced efficacy. Moreover, the drugs that are used in wound dressing tend to have poor solubility which makes penetration into wounds difficult (Mordorski *et al.* , 2015). New strategies are focusing on the incorporation of NPs to develop wound healing agents that allow for a more targeted drug delivery approach. There are two ways in which NPs can be used in wound healing; NPs possess intrinsic characteristics which aid wound healing and can also be used as delivery vehicles for therapeutic agents (Mihai *et al.*, 2019). The NPs have a large surface area to volume property which can increase their likelihood of interaction with therapeutic molecules. Nanofibers can also be used as wound dressings to facilitate collagen synthesis and re-epithelization of wounds (Shahverdi *et al.*, 2014).

The use of NPs as drug delivery will allow for the stabilization of previously unstable or poorly soluble drugs to improve the efficacy of traditional dressings. AgNPs are among the MNPs that have been incorporated into wound dressings due to their antibacterial and anti-inflammatory properties (Nqakala *et al.*, 2021). These NPs have been evaluated successfully on chronic wounds (Dowsett, 2004). However, AgNPs pose a threat to human health and the environment and further research is required to ensure safety in the clinical implementation of these NPs (Paladini & Pollini, 2019). The AuNPs are now attracting a lot of interest as potential wound healing agents. This is sparked by the ease of synthesis, chemical stability, and the capacity of AuNPs to absorb light near the infrared region (Niska *et al.*, 2017).

1.2.2 AuNPs

AuNPs are referred to as colloidal gold when diluted in water (Yeh *et al.*, 2012) and range in size from 1 to 100 nm (Rai *et al.*, 2016). The AuNPs exhibit intense absorbance and scattering incident light at its SPR. These are the most stable NPs and can be synthesized by various techniques such as pioneer Turkevich and Brust method. They can be classified into nanowires, nanorods, nanospheres, nanocubes, nanoshells among others based on their shapes (Li *et al.*, 2014). Due to their size-related optical and electronic properties, as well as their biocompatibility and non-cytotoxicity, their application in medicine and biophysical research continues to increase significantly (A. K. Khan *et al.*, 2014). The biocompatibility of gold has resulted in the long history of its application in the treatment of cancer and arthritis (S. Wang & Lu, 2018) and influenced the use of AuNPs in biomedical applications. Gold is an inert metal with good thermal and electrical conductivity. It is used in electric devices, dentistry,

and medicine. Gold is considered inert; however, its NPs counterpart raises a lot of concerns as they might exhibit unique activities. Despite these uncertainties, AuNPs are versatile and can be tuned to suit various research as imaging and diagnostic tools and tumour treatment, as a result, there is a large demand for their production on a large scale (Harish *et al.*, 2022).

Noble metals are of particular interest due to their close-lying conduction and valence bands in which electrons move freely (Raveendran *et al.*, 2003). In an aqueous solution, the interaction of AuNPs with light depends on their shape, size, and environment. The AuNPs at ~30nm absorb the light around the ~450nm (blue-green) of the spectrum and reflect a red colour (Merck, 2022). As the size of the NPs increase, the SPR shifts to the red light, and a purple-blue light is reflected. Numerous applications favour NPs of the same size hence mono-dispersed NPs are preferred over poly-dispersed NPs.

1.2.3. Methods of AuNP synthesis

NPs can be synthesized by a top-down or bottom-up approach as shown in **Figure 1.2** and these classes can be further divided based on the protocols and operation or conditions of the reaction (Lee & Jun, 2019).

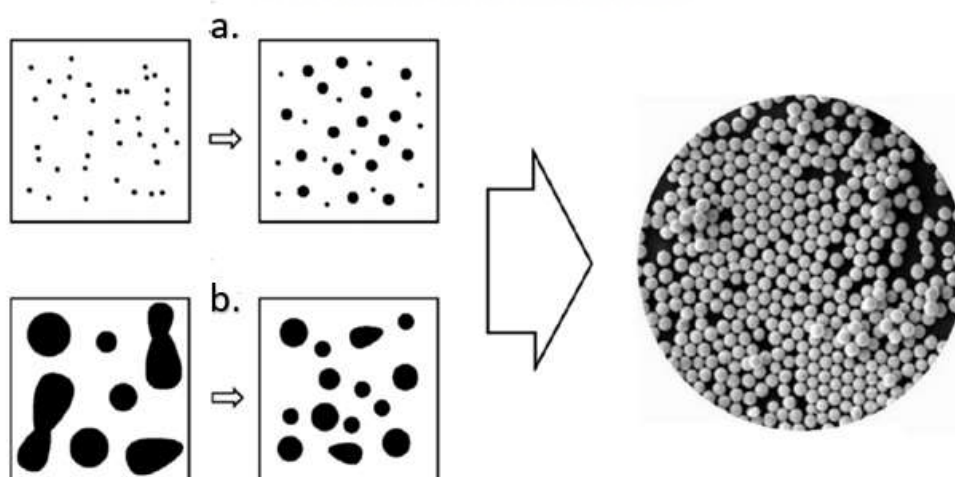


Figure 1.2: The bottom-up (a) and top-down (b) approaches for synthesis of NPs. Reprinted with permission from the American Chemical Society (Y. Wang & Xia, 2004).

The top-down method employs destruction or decomposition methods to reduce bulk materials into smaller, nanometric scale units, these smaller units are further decomposed to NPs. The decomposition methods include laser ablation, thermal decomposition, grinding and chemical vapor deposition. Among these various methods, mechanical milling is the most common, where different elements are milled in an inert atmosphere (Ealias *et al.*, 2017).

The bottom-up approach is the build-up of NPs by chemical or physical methods from relatively smaller substances by reduction or sedimentation. Examples of this approach are sol-gel, spinning, biochemical, and green synthesis (Iravani, 2011). Various physical and chemical methods are used in the production of AuNPs, such as the Turkevich, and the Brust-Schiffrin methods. Also known as the citrate reduction, the Turkevich method (Zhao & Friedrich, 2015) is a classic convenient and popular method due to ease of synthesis, simplicity, and stability of the resulting NPs is, however, a limiting factor. In the Brust method, sodium borohydride (NaBH_4) is used as the reducing and stabilizing agent. NaBH_4 reduces AuCl_4^- in a two-phase reaction and the resulting AuNPs have sizes ranging between 1 and 3 nm (Slepička *et al.*, 2020).

These methods are often expensive and require the use of toxic reducing and stabilizing agents which can be detrimental to human health and the environment. Preference has therefore been given to alternative environmentally friendly methods which use natural products as reducing and stabilizing agents in green nanotechnology. The reference guide for scientists and researchers in the synthesis of NPs via green chemistry is in accordance with the green chemistry principles. The key factors in the preparation of NPs using green chemistry include the choice of solvent, choice of environmentally friendly reducing and stabilizing agents) to produce non-toxic products (Raveendran *et al.*, 2003). The inspiration for the green approach is motivated by the use of natural products and researchers are hoping to replicate nature's ability to produce small clusters of atoms that can self-assemble to more elaborate structures.

1.2.3.1 Green synthesis of MNPs

In the green chemistry approach, the bio-reduction process takes place at neutral pH, low synthesis temperature, and uses non-toxic reducing agents (Anastas & Eghbali, 2010). It has recently been discovered that biological materials such as fungi (Moghaddam *et al.*, 2015), plants and (Korde *et al.*, 2020);(Makarov *et al.*, 2014), and bacteria (Tsekhmistrenko *et al.*,

2020) can be used to transform the ions of inorganic metals into MNPs. Plant materials such as peel, fruit, stem, roots, and micro-organisms such as bacteria, yeast, fungi, and actinomycetes can be used in the biosynthesis of AuNPs (Ahmed, Annu, *et al.*, 2016). Synthesis occurs in a single step and produces NPs that are stable with diverse morphologies. The mechanism of the biosynthesis of NPs from plants is based on the phytoremediation ability they possess. Plants have been used in the extraction of metals from biomass to return an economic profit (Ahmed, Annu, *et al.*, 2016). The main objectives of biosynthesis are the reduction of hazardous waste and ensuring efficiency. Such a non-hazardous synthesis exhibits superiority over the former methods.

(i) Biosynthesis of AuNPs from micro-organisms

Microorganisms such as fungi, bacteria, and algae are capable of producing NPs. The general interpretation of the production of NPs from microorganisms is that some of the enzymes present in these organisms can reduce metal ions into MNPs. Various microbes have been reported for synthesizing Au and Ag NPs (Rónavári *et al.*, 2021) examples of microorganisms that can be utilized in the synthesis of MNPs include *Lactobacillus kimchicus* (Aziz Mousavi *et al.*, 2020) and *pseudomonas aeruginosa* (Abd El-Aziz *et al.*, 2007).

The enzymes produced by metabolic processes in microorganisms such as fungi, bacteria, actinomycetes, and yeast can be used to reduce metal ions to MNPs (Moghaddam *et al.*, 2015). The synthesis of NPs by the enzymatic process is a 'green' approach as it is not energy-intensive, microbes grow in low-cost environments and are easy to maintain. Depending on the location where the synthesis occurs, synthesis by microbes can be classified as intracellular or extracellular method (X. Li *et al.*, 2011). The former involves the transportation of the metal ions into the cell, and in the latter, the synthesis occurs on the surface of the cell. In intracellular mechanism, the positively charged ions are transported into the negatively charged cell wall where they are diffused to their ground states by electrostatic force and in extracellular synthesis, this is mediated by enzymes such as hydroquinone or the nitric reductase (Rónavári *et al.*, 2021). The quality of NPs synthesized from microorganisms is known to depreciate over time, so their stability needs to be studied further to enhance it.

(ii) Biosynthesis of AuNPs using plants

Plants consist of metabolites such as sugars, proteins, polyphenols, alkaloids, and terpenoids that play a role in the reduction of metal ions into MNPs. Flavonoids, for example, are a large group of polyphenols that can reduce these ions. The mechanism of the conversion of the ketone to carboxylic acid in flavonoids is involved in Au³⁺ reduction to Au⁰ (Makarov *et al.*, 2014). During the tautomeric transformation of flavonoids from the enol-form to the keto-form, reactive hydrogen may be released that can reduce metal ions into MNPs, this type of reaction is also common in the Ag⁺ reduction (Ahmed *et al.* 2016).

Plant-mediated synthesis of AuNPs can be classified as *in vivo* and *in vitro* methods. In the *in vivo* method, plants can reduce metal ions on their surface, tissues, or various organs remote from the ion penetration site. The *in vitro* process of synthesizing NPs can be achieved by using plant extracts obtained from different plant parts such as stem, stalk, leaf, roots. Plants contain metabolites such as polyphenols, sugars, proteins, and alkaloids which play a role in the reduction of metallic gold to AuNPs and ensure the stability of the NPs (Li *et al.*, 2014). The plant materials upon collection are washed with deionized water and dried. The dried materials are crushed or blended to form a powder which is then extracted in water. The solution is purified by filtration and is freeze-dried or rotary-vapor to obtain powdered samples. Different concentrations of gold salt are mixed with the extracts and usually, a colour change to a wine-red will indicate the formation of AuNPs (Barry, 2019).

Biosynthesis of AuNPs using plants products

(iii) Mechanism for the biosynthesis of AuNPs from plants

Although the mechanism for the synthesis of AuNPs from biological agents is not clearly known the chemical compounds present in the plant extracts may act as reducing agents. This reaction will lead to the reduction of metal ions thereby forming MNPs as shown in **Figure 1.3** There are three main phases in the mechanism of the synthesis of AuNPs from plant extracts. In the initial stage, the metal ion binds to the reducing and stabilizing agents and is reduced to metal atoms, this is the activation stage. This is followed by the growth phase, also known as the Ostwald ripening, the merging of small NPs to form larger NPs. The final stage is the termination stage, this stage determines the shape and size of the NPs (Y. C. Wang & Gunasekaran, 2012).

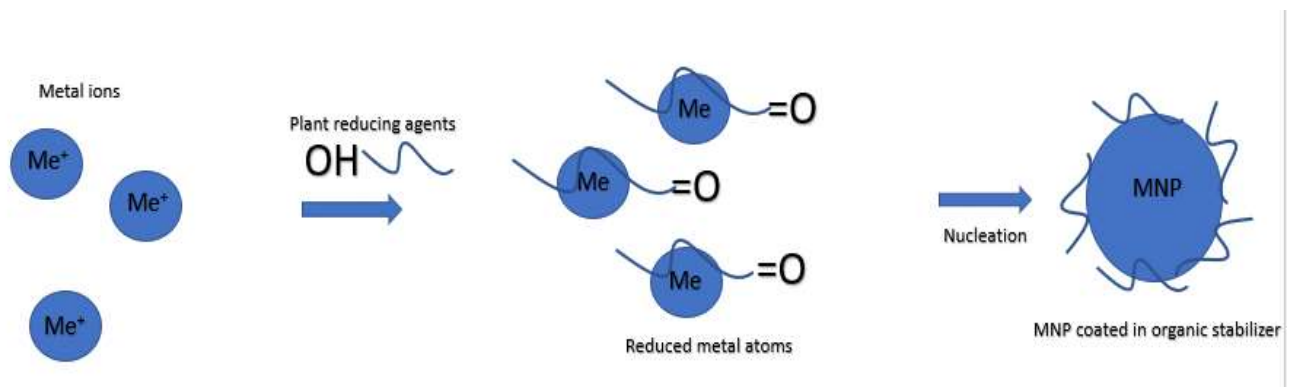


Figure 1.3 Mechanism for the synthesis of MNPs using plant extracts as reducing and stabilizing agents. (Moodley *et al.*, 2020)



1.2.4 Applications of AuNPs

AuNPs have a wide range of applications as they are versatile and have many advantages compared to other nanocarriers. This growing interest in the potential of these AuNPs in research arises from their tuneable physiochemical properties, some of their applications are summarized in **Table 1.2**.

Table 1.2: Applications of AuNPs

Applications	Short Description	Reference
Diagnostics	AuNPs can be used as biosensors in the diagnosis of cancer, heart, and infections. The threshold of detection is reduced using highly sensitive AuNPs.	(Peng <i>et al.</i> , 2009)
Therapeutic drug delivery	Therapeutic agents can be coated onto the surface of AuNPs.	(A. K. Khan <i>et al.</i> , 2014)
Photodynamic therapy	When excited by light in the wavelengths 700nm – 800nm, near IR absorption, AuNPs produce heat (hyperthermia) that can be used to eradicate tumours.	(Stuchinskaya <i>et al.</i> , 2011)
Electronics	Can be used as conductors in electrical devices	(Sousa <i>et al.</i> , 2017)
Catalysts in chemical reactions	AuNPs can catalyse certain reactions. They can reduce some reactions (NaBH_4) and their surface can be used for selective oxidation.	(Thompson, 2007)
Substrates in Raman spectroscopy	AuNPs as substrates can be used in the measurement of vibrational energies of chemical bonds	(Shamsaie <i>et al.</i> , 2007)

1.2.4.1 AuNPs for Drug delivery

When chemotherapeutic drugs are administered traditionally (orally or by injection), the drugs diffuse and only a fraction of the drug reaches the tumor site. This convectional method requires high doses (Senapati *et al.*, 2018). Irradiation, chemotherapy, and surgery are also used in the treatment of cancer, but these methods have their shortcomings. These treatment methods are non-specific and can damage the surrounding healthy cells when employed. The conjunction of drugs with AuNPs seeks to minimize these effects. The AuNPs can be used in targeted drug delivery at the tumor or disease site to improve the solubility as well as the uptake as they are generally characterized by a high surface area to volume ratio. The goal of

AuNPs in drug delivery is to improve the bioavailability of drugs at the diseased or tumor site to increase drug efficacy and to decrease the negative effects of these drugs on the normal tissues (F. Li *et al.*, 2020). Particles in nanoscale can effectively penetrate through cellular barriers as they travel through blood capillaries into the individual cells (Barua & Mitragotri, 2014).

AuNPs, as drug delivery systems, have unique optical properties giving them an advantage over other nanocarriers and conventional drug delivery methods. These NPs can be used to transport vaccines, drugs, proteins, or nucleotides by direct conjugation into the AuNP surface by either physical adsorption or covalent bonding. These materials can then be released by internal (pH, enzyme sensitivity, or redox) or external (light, heat, or magnetism) stimuli (Li *et al.*, 2007). Kong *et al* established that the carboxylic groups on methotrexate, an anti-cancer drug, can attach to the surface of AuNPs when incubated overnight and this conjugation increases the concentration of methotrexate on target cells (Lundgaard *et al.*, 2018). The AuNPs are promising in drug delivery; however, their long-term cytotoxicity needs to be evaluated before clinical application (Sibuyi *et al.*, 2021).

1.2.4.2. The AuNPs for wound healing

The AuNPs have shown intrinsic properties that can aid in wound closure by enhancing cell growth and have been used as drug vehicles for drugs commonly employed in wound therapy. The AuNPs have received attention due to their chemical stability and ease of synthesis. During the wound healing process, molecular mediators such as reactive oxidative species (ROS), neutrophils, and inflammatory cytokines are released (Eming *et al.*, 2007). ROS is released as a by-product of cellular metabolism and excess amounts can be detrimental to the wound healing process. The AuNPs can act as antioxidants and prevent the production of ROS and promote wound healing (Mihai *et al.*, 2019).

One of the best innovative techniques was to incorporate the AuNPs into existing ointments that are used in wound healing. A previous study reported on the bio-reduction and synthesis of AuNPs, AgNPs, and Ag/AuNPs from an extremophilic actinobacterium *Streptomyces sp.* Ointments were prepared by adding 4.50g of 0.2% w/w Nitrofurazone petroleum jelly and 10% NPs used for topical application. In comparison to standard ointment treatment, the ointments containing the NPs healed 100% of the wounds in 19 days instead of 21 days in control animals (Shanmugasundaram *et al.*, 2017). This shows that green nanotechnology is

able to modify technologies that are currently being used to increase their efficiency as well as develop novel strategies that have improved properties. The main advantage of using green synthesis is that the cost of development and end products can be significantly reduced. The synthesis of AuNPs is cost-effective, and time-efficient especially when plant materials are used (Shah *et al.*, 2015) .

Plant-synthesized AuNPs have shown potential wound healing properties, they have been used as an antibacterial, growth enhancer, antioxidant agent (Boomi *et al.*, 2020). Recently, AuNPs synthesized from different African plants were investigated for their potential in wound healing. The AuNPs synthesized by Elbagory *et al* exhibited antibacterial activity against Gram-positive and Gram-negative bacteria. This is an especially critical property for the healing of chronic wounds. The AuNPs synthesized from African *Galenia Africana* and *Hypoxis hemerocallidea* plant extracts were found to possess anti-inflammatory activities and reduced the levels of the cytokines, IFN- γ in natural killer cells exposed to these AuNPs (Elbagory *et al.*, 2016). Similar results were obtained when the secretion of proteins involved in wound healing from AuNPs purchased from a NanoTrade Ltd company (the Czech Republic, est 2004), was evaluated on NHDF cells by scratch assay. Results showed a decrease in the production of the pro-inflammatory cytokines, interleukin-6 (IL-6), IL-12, and tumour necrosis factor-alpha (TNF- α), and proteins involved in angiogenesis suggesting anti-inflammatory and anti-angiogenic activity of AuNPs (Pivodová *et al.*, 2015).

Burns and wounds can be frequently colonized by bacteria that proliferate in the exposed tissues and when established, these bacteria can pass through the blood capillaries of the tissues, and eventually lead to bacteremia. An ointment with AuNPs will decrease the bacterial load and thus prevent infections. The effect of negatively charged surface AuNPs on wound healing was investigated by Pivodova *et al.* This study evaluated the viability of normal dermal fibroblasts and normal human epidermal keratinocytes and the results showed that the AuNPs were not toxic to these cells (Pivodova *et al.*, 2015). The interaction of AuNPs with skin cells is a crucial area in biological research. Little is known about the toxicity of AuNPs when in contact with the biological systems and needs to be evaluated *in vitro*.

1.2.5 Wound healing effect of RW-AuNPs

1.2.5.1 Wine classification and phytochemical composition

Wine is an alcoholic beverage produced from the fermentation of grapes, *Vitis vinifera*. Wine can be classified into three categories: white, red or rose. The factors such as alcohol content, sweetness, colour, grape variety, fermentation process, maturation, and origin of the grape, determine the type of wine that is produced. White wines are obtained from the fermentation of grape juice (Ribéreau-Gayon *et al.*, 2006) but RWs are obtained by the alcoholic fermentation of squeezed grape skin or the seeds. The phenol compounds in RWs are known to be 10-fold more than that of white wines, attributed to their more antioxidants compared to white wine. Pinot noir (PN) contains the highest number of antioxidants compared to any other RWs (Elangkovan & Ganapathy, 2020).

The difference in colour between red and white wines is due to the different phenolics present in beverages. The simple phenolics; hydroxybenzoic and hydroxycinnamates are found in the flesh of the grape but the other more complex phenolics, also known as flavonoids, are found in the skin, seeds, stalk, and, roots. Flavonoids are common in the pomace (skin, stem, and pulp), which is used in the production of RWs hence the red colour. (The International Wine of the Month Club, 2022).

An average wine consists of about 86% water, 12% ethanol, 1% glycerol, 0,4% organic acids, and 0,1% tannins and phenols. The remaining 0,5% is comprised of volatile compounds (such as mineral anions and cations). The exact percentages differ with the type of wine.

The health benefits and phenols of interest present in RW are flavonoids. These polyphenolic compounds are widely distributed in the plant kingdom and are widely used in medicine for the maintenance of capillary integrity due to their anti-inflammatory, anti-ulcer, anti-hepatotoxic properties (Bors *et al.*, 1990). Structurally, flavonoids have two phenolic rings and an oxygenated heterocycle. This class of phenols is found in a variety of plants and is sub-divided into four classes; Tannins, Catechins, Anthocyanins, and Resveratrol (Pandey & Rizvi, 2009).

(i) Tannins

Tannins are water-soluble polyphenols also referred to as tannic acid (Chung *et al.*, 1998), they are subdivided into two classes: condensed and hydrolyzed. The most abundant being

the condensed. The condensed tannins are polymers of flavanone-3-ol subunits, mainly found in RW as they occur in the skin or seeds of the grape. Tannins give the wine its bitterness and acidity, the dry sensation obtained from drinking RW arises from the reaction of proteins in a person's saliva and the tannins. Due to their antioxidant activity, they are associated with health benefits (Amarowicz, 2007)..

(ii) Catechins

Catechins are naturally occurring polyphenolic phytochemicals found in medicinal plants and food. These phytochemicals have well demonstrated antioxidant activity (Zheng *et al.*, 2008). This group forms a large part of wine, and they possess antimicrobial, anticarcinogenic, and antioxidant properties. Structurally, catechins consist of two benzene rings and a dihydropyran heterocycle with a hydroxyl group attached to C3 (Singhal & Saxena, 2015).

(iii) Anthocyanins

Anthocyanins are bioactive water-soluble phenolic compounds that occur naturally (Riaz *et al.*, 2016). They are also found in the skin of the grape; they contribute to the coloration of red grapes. These compounds are strong antioxidants as demonstrated *in vitro* using cell lines derived from the colon, epithelial, keratinocytes (L. Wang & Stoner, 2008).

(iv) Resveratrol

Resveratrol is a naturally occurring polyphenol of the stilbene family produced in regularly consumed plants such as berries, grapes, and peanuts in response to infections and stress within their environments such as fungal infections, injury, and harmful radiation. Scientific interest is sparked by the antioxidant and free radical scavenging properties of resveratrol which support that wines, have health benefits. Resveratrol can promote circulation, prevent premature aging, protect against diabetes and cancer (Maggiolini *et al.*, 2005). In cancer tumors, it can inhibit the initiation, promotion, and progression of the tumor cells (Bader *et al.*, 2008).

1.2.5.2. Synthesis of AuNPs from grape products.

Wine is envisioned to be the best option to produce NPs due to the alcohol, sugar, and anthocyanins as opposed to the grape itself (Krishnaswamy *et al.*, 2014). The potential of grape skin, stalk, and seeds obtained from grape processes to produce the AuNPs was studied

previously (Amarnath & Mathew, 2011). RW offers a variety of health benefits and has a chemical composition comprising of ethyl sugars, polyphenols, and organic acids.

Resveratrol is one of the polyphenols present in RW that is passed on from grape seeds and skins to the wine during production. This substance possesses anti-inflammatory, antioxidant, and cardioprotective properties. When one consumes these plants, they can acquire similar protection, hence it is known to have health benefits to humans. Fermented grape juice (Dzimitrowicz *et al.*, 2017), grape pomace (Baruwati & Varma, 2009) and RW (Pavliashvili *et al.*, 2017) have all been used in the synthesis of AuNPs but due to the high solubility in alcohol, resveratrol was found in abundance in RW which basically means a person's body can absorb large amounts from RW than any other source. However, the intake of will be regulated as alcohol itself is neurotoxic. The prolonged intake affects the central nervous system (Lundgaard *et al.*, 2018).

1.2.5.3. Synthesis of AuNPs from fermented grape juices

Fermented grape juices were used as reducing and capping agents for the biosynthesis of spherical AuNPs. The AuNPs were produced using four fermented grape juices; a semi-sweet red (I), semi-dry red (II), semi-sweet white (III), and dry white (IV) fermented grape juices. Due to the low phenolic concentration amount in white grapes, the expected and thus obtained results from an LSPR band show symmetrical peaks for I and II but III and IV there was far less symmetry (Dzimitrowicz *et al.*, 2017).

1.2.5.3. Synthesis of AuNPs from grape pomace.

The potential of grape skin, stalk, and seeds obtained from grape processes to produce the AuNPs have been reported. This was done in a single-step method using water at room temperature. A simple cost-effective procedure produced AuNPs that was stable with an extended shelf life (Amarnath & Mathew, 2011). It was previously demonstrated that using water as a solvent in chemical reactions as compared to organic solvents is recommended (C. J. Li & Chen, 2006). The water-dispersible nature of AuNPs from grape by products along with its inherited health benefits can revolutionize the impact of nanotechnology on biomedical applications.

Some studies used the red grape pomace as a three-in-one reagent because it contains numerous polyphenolic compounds which could act as capping and reducing agents during the synthesis process. Phenolics and to a lesser extent, the reducing sugars were identified to

play a significant role in the reduction and stabilization of the AuNPs (Dzimitrowicz *et al.*, 2017) which shows the great potential of red grapes as bio-reducing agents in the green synthesis of AuNPs (Nadagouda & Varma, 2008). The use of pomace as a reducing agent and capping agent instead of wine, led to large-scale production and at the same time has the benefit of utilizing an industrial waste with high biological and oxygen demand (Hoag *et al.*, 2009).

Grape wine and grape pomace extracts were shown to reduce AuNPs using a 50W of microwave power, in this study individual components of the grape pomace were isolated and used to synthesize AuNPs in water at room temperature. The grape pomace such as seeds, skin, and stalk contain proanthocyanins, a rich source of natural antioxidants with health benefits against cardiovascular diseases. Since this is an eco-friendly method, it supports the concept of synthesizing AuNPs by the polyphenolic compounds present in grape extracts, like wine and it also suggests that other foods waste materials that are rich in polyphenols can be potentially converted into high-value nanoproducts.

1.2.5.4 Synthesis of AuNPs from RW

Wine is envisioned to be the best option to produce NPs due to their high alcohol, sugar, and anthocyanin content as opposed to other grape products. As it is well known, the properties and flavors of wine depend on factors such as place of growth, climate, the grape variety, and the technology involved in making the wine (Styger *et al.*, 2011). The process of producing AuNPs from chloroauric acid by using the RW Saperavi was discussed (Pavliashvili *et al.*, 2017). This type of wine is made from a pinot noir (PN) grape that has thick skin, which suggests that the amount of resveratrol will be high. Saperavi grapes are grown in an eponymous local grape cultivar in the province of Kakheti in Georgia (USA). The synthesis was carried out at room temperature in an aqueous solution of chloroauric acid. The wine was poured into a flask in small portions with the working electrode. The PN wine was used simultaneously as a reducing agent and stabilizer of the AuNPs (Pavliashvili *et al.*, 2017). Although studies have shown that RW can produce AuNPs, their wound healing activity has not been reported as yet.

1.3 Aim of the study

This study aimed to synthesize AuNPs from an RW-Es through green chemistry and to investigate the effect of these AuNPs in wound healing.

1.4 Objectives

- To prepare wine extracts from P, PN, and CS RWs
- To synthesize AuNPs from the RW-Es
- To determine the stability of the RW-AuNPs in different buffers.
- To characterize the RW-AuNPs by UV-Vis, Zeta-Sizer, FT-IR, TEM, and DLS.
- To evaluate the antioxidant activity of the RW-Es and RW-AuNPs using the DPPH assay
- To evaluate the effect of the RW-Es and the RW-AuNPs on KMST-6 cells using MTT assay
- To determine the efficacy of RW-AuNPs in wound healing using the scratch assay.



CHAPTER 2: MATERIALS AND METHODS

2.1 Materials

Table 2.1: List of chemicals

Chemicals	Suppliers
2,2-diphenyl-1-picrylhydrazyl (DPPH)	
3-(4,5-Dimethylthiazol-2-yl)-2,5-diphenyl-2H-tetrazolium bromide (MTT)	
Ascorbic acid (AA)	
Chloroauric acid (gold salt)	
Cisplatin	Sigma-Aldrich
Gallic Acid (GA)	
Sodium Carbonate (Na ₂ CO ₃)	
Sodium Hydroxide (NaOH)	
Trypan Blue	
Trypsin-EDTA	
Dimethyl Sulphoxide (DMSO)	
Ethanol (EtOH)	Kimix
Methanol (MeOH)	
Dulbecco's Modified Eagle Medium (DMEM)	
Penicillin streptomycin (pen-strep)	Lonza
Phosphate Buffered Saline (PBS)	
Fetal Bovine Serum (FBS)	Thermo Fischer Scientific



Table 2.2: List of instruments

Instrument and Manufacturer	Country of the Manufacturer
Adventurer Vhaus balance	China
BUCHI Rotavapor R-114	Switzerland
Eppendorf centrifuge 5417R	Germany
Eppendorf thermomixer comfort	Germany
EVOS XL core	USA
LABotec Thermo electron corporation incubator	USA
Invitrogen Countess™ automated cell counter	Korea
PerkinElmer spectrum two	UK
BMG labtech POLARstar omega plate reader	Germany, Europe
Sorvall TC centrifuge	USA
XS pH meter Wissam	China
Malvern Zetasizer ZS90 Nano series	United Kingdom

Table 2.3: Cell line

Cell line	Species	Source	Media
KMST-6	Human	Skin Fibroblast	DMEM

2.2 Methodology

2.2.1 Preparation of RW extracts (RW-Es)

Three RWs: Van Loveren *Pinot Noir* (PN), Van Loveren African Java *Pinotage* (P), Coral Reef *Cabernet Sauvignon* (CS), were purchased from Checkers liquors Parow (Parow Centre Mall, Cape Town, SA). An aliquot of 500mL of each of the RWs was transferred into a round bottom flask and the alcohol was dried by a rotary evaporator (BUCHI Rotavapor) at a temperature of 50°C for 6 hrs. The resulting paste was dried in a 70°C oven overnight. A

100mg/mL stock solution of the RW-Es was prepared in deionized water and stored at 4 °C until further analysis.

2.2.2 Synthesis and characterization of RW-AuNPs

2.2.2.1 Optimization of synthesis conditions

RW-AuNPs synthesis was optimized by varying the temperature, RWE concentration, chloroauric acid concentration, pH, and time as previously described with some modifications (Elbagory *et al.*, 2016); (Dube *et al.*, 2020). The AuNP formation was confirmed by colour change, UV vis, and DLS analyses.

(i) Effect of temperature and RWE concentration on the AuNP synthesis

The 100mg/mL stock solutions of the RW-Es were serially diluted to obtain 50mg/mL; 25mg/mL ; 12.50mg/mL ; 6.25mg/mL ; 1.125mg/mL concentrations. Then, 0.04mL of each solution was added into a 1.5mL tube containing 0.36mL of preheated 1mM chloroauric acid at 1:9. The reactions were carried out on an Eppendorf Thermomixer at one temperature (25°C, 30°C, 50°C, and 100°C) at a time while observing a colour change from 0 - 1 hr while shaking at 1000rpm.

(ii) Effect of gold salt concentration on the AuNP synthesis

To determine the optimal gold salt concentration, various concentrations of gold salt (0.25, 0.5, 0.75, 1, 2, 3, 4, and 5 mM) were prepared and used in the synthesis of AuNPs at the optimal RWE concentration and temperature. Synthesis was carried out as described above.

(iii) Effect of RWE pH on the AuNP synthesis

Following optimization of the synthesis temperature and RWE concentration, the effects of RWE pH were evaluated. Briefly, 4mL of the RWE stock solutions at 25mg/mL was adjusted to pH 4, 5, 6, 7, 8, 9, and 10 by the addition of concentrated NaOH. The pH solutions were then adjusted to a final volume of 5mL by an addition of deionized water. The resulting solutions were added to the preheated gold salt solution and the reaction was performed at the previously optimized RWE concentration, gold salt concentration, and temperature as described above.

2.2.3 Reaction Kinetics

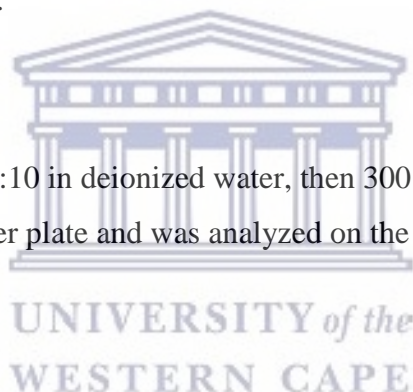
The kinetics of the bio-reduction of RW-AuNPs was monitored by UV-Vis at the established optimal reaction parameters. The UV-Vis readings were measured between 0 and 240mins and the λ_{max} at each time point was plotted against time using OriginPro v8 software (OriginLab Corporation, Northampton, Massachusetts, USA).

2.3 Characterization of the AuNPs

The RW-AuNPs were centrifuged on an Eppendorf centrifuge 5417R for 5 min at 10 000rpm at room temperature for 5 minutes. After centrifugation, the supernatant was discarded, and the pellets were resuspended in the same volume of deionized water and kept at room temperature for further analysis and applications. The RW-AuNPs were characterized using UV-Vis, DLS, FTIR, and TEM.

2.3.1 UV-Vis Analysis

The RW-AuNPs were diluted 1:10 in deionized water, then 300 μl of the AuNPs was added in a 96-well Flat-Bottom Greiner plate and was analyzed on the POLARstar Omega plate reader at 300 - 1000 nm.



2.3.2 DLS analysis

To determine the hydrodynamic size and the polydispersity index (PDI), 1mL of the washed RW-AuNPs was added into a polystyrene cuvette for size and PDI. The samples were analyzed by the Malvern Nano ZS90 Zetasizer.

2.3.3 FT-IR Spectroscopy analysis

A small quantity of the dried RW-AuNP samples and KBr were mixed in a ratio of 1:99 and placed in a mortar and crushed using a pestle (Oh & Chun, 2019) . The resulting fine powder was inserted into the pellet compressor and placed into the PerkinElmer spectrum two spectrometers FT-IR instrument. Prior to sample analysis, KBr powder was crushed and analyzed as a background reference. All the samples were analyzed between 4000cm^{-1} and 400cm^{-1} wavenumber.

2.3.4 *In vitro* stability test

The stability of the RW-AuNPs was evaluated in different solutions for 24 hrs. The RW-AuNPs were centrifuged as before, the pellets were resuspended in 2mL of test solutions (water, phosphate-buffered saline (PBS), 10% fetal bovine serum stain buffer (FBS), and Dulbecco's modified eagle medium (DMEM)), and incubated at 37°C for 0-24hrs. The UV measurements were taken at 1hr intervals for the first 6hrs and at 24hrs to monitor possible changes in the UV-vis spectra of the RW-AuNPs (Elbagory *et al.*, 2016).

2.3.5 Quantification of RW-AuNPs by ICP-OES

To determine the concentration of RW-AuNPs in solution, 2mL of AuNPs was centrifuged at 14000rpm for 5min at room temperature. The RW-AuNP pellets were then resuspended in 2mL Aqua regia in a 15mL conical tube. The solution was digested in a 90°C oven for 2hrs and thereafter diluted to 10 mL with 2% HCl as previously described (Nicole Remaliah S Sibuyi *et al.*, 2017). The samples were analyzed using ICP-OES at the Chemistry Department (UWC).

2.3.6 Antioxidant Activity of RW-Es and AuNPs: DPPH assay

The antioxidant activity of the RW-Es and RW-AuNPs was evaluated according to previously described protocol (Stozhko *et al.*, 2019). The DPPH stock solution was prepared by dissolving 1,4mg of DPPH in 12mL of 99% ethanol to a final concentration of 0,30mM. Six concentrations of each RW-Es (PN, P and CS extracts) and their respective AuNPs at 0.10, 0.15, 0.20, 0.25, 0.30 and 0.35mg/mL were tested. Ascorbic Acid (AA) was used as a positive control at the same concentrations. In a 96-well plate, 160µl of 0,30mM DPPH followed by 40µl of each sample was added to each well. All the samples were added in triplicate and the experiment was repeated thrice. The plate was incubated in the dark at 37°C for 60min. Absorbance for all the samples was measured at 517nm against ethanol blank, and used for the calculation of the percentage inhibition as follows:

$$\% \text{Inhibition} = \frac{A_{\text{control}} - A_{\text{test}}}{A_{\text{control}}} \times 100$$

Where A_{control} is DPPH + ethanol and A_{test} is DPPH + sample.

% Inhibition was plotted against sample concentration and the IC₅₀ values were extrapolated.

2.4 Effect of RW extracts and AuNPs on cell viability

2.4.1. Cell Culture

Frozen KMST-6 cells in 2mL cryovials were retrieved from -120°C and thawed at room temperature. The cell suspensions were then transferred into a 15 mL tube containing 5 mL complete DMEM (DMEM containing 1% penstrep and 10% FBS) and centrifuged in a Sorval TC centrifuged at 3000rpm for 5min. The supernatant was discarded, and the cell pellets were resuspended in 5mL complete DMEM and transferred into a T25 cell culture flask. The cells were grown at 37°C in a humidified 5% CO₂ Thermo electron corporation incubator, and the media was changed every three days until the cells reach at least 70% confluency.

2.4.2. Trypsinization of the cells

When the cells reached 70-90% confluency, the media was removed from the flasks and the cells were washed with 2mL PBS. Then, 4mL of trypsin-EDTA was added to the flasks and incubated for 5min in a 37°C incubator and observed under the EVOS XL core light microscope to ensure all cells have detached. The detached cells were transferred into a 15mL conical tube and 12mL of complete DMEM was added to stop the effect of trypsin. The cells were centrifuged at 3000rpm for 5min, and the supernatant was discarded. The pellets were resuspended in 1mL complete DMEM.

2.4.3. Trypan blue dye exclusion assay

The cell count assay was performed using Trypan blue dye exclusion assay following a previous protocol (Strober, 2001). The cell suspension (10µl) was mixed with 10µl of 0.4% trypan blue solution and the solution was loaded onto a Countess cell counting slide. The cells were counted on the Countess™ automated cell counter.

2.4.4. Storage of cells

After trypsinization, the cells were resuspended in complete DMEM. Cell count was performed as before using Trypan blue dye exclusion assay (2.4.2). Cells at 1x10⁶ cell density were prepared in complete DMEM containing 10% DMSO. The cell suspension was aliquoted into 2mL cryovials and stored in a -120°C freezer.

2.4.5. Effect of RW-Es and RW-AuNPs on cell viability: MTT assay

KMST cells (100µl/well) at a cell density of 1×10^5 cells/mL⁻¹ were seeded onto a sterile 96-well F-bottom plate and incubated for 24hr at 37°C in a humidified 5% CO₂ Thermo electron corporation incubator. After 24hrs incubation, the cells were treated with 100µl of DMEM containing RW-Es and RW-AuNPs at concentrations ranging from 0.005 to 1mg/mL and 1.56µg/mL - 50µg/mL, respectively. Cisplatin (1µg/mL) was used as a positive control and untreated cells were used as a negative control. Treatments for RW-Es were done in triplicates, and the RW-AuNPs treatments were done in quadruplicates. One of the wells for cells treated with RW-AuNPs was used to account for interference. After 24h of incubation, the treatment was removed and replaced with 100µl of 1:10 dilution of MTT (5mg/mL stock concentration) solution prepared in fresh media, and the plate was covered in foil and incubated for 3hrs at 37°C. For the interference test, media without MTT dye was added to the cells. The MTT was replaced with 100µl of >99,5% DMSO, and the plate was further incubated for 30mins. The absorbance was read at 570 and 700 nm on a PolarSTAR Omega plate reader. The percentage cell viability was calculated using the optical density obtained as follows:

$$\% \text{Cell viability} = \left(\frac{\text{mean untreated}}{\text{mean treated}} \right) \times 100\%$$

2.5. Scratch Assay

The *in vitro* scratch assay was performed on KMST-6 cells to evaluate the effect of treatments on cell migration following a previous protocol (Nqakala *et al.*, 2021). The cells were prepared and counted as before, then 500µl of 2×10^5 cell/mL were seeded onto a 24 well sterile plate and incubated for 24hrs at 37°C. After 24hrs, the media was removed and replaced with 1mL of PBS to remove floating cells.

Using a sterile 200µl pipette tip, the well was scratched across the center and another line, perpendicular to the initial scratch was drawn to make a cross. The PBS was removed along with the detached cells and the cells were treated with 50µg/mL of RW-AuNPs prepared in DMEM supplemented with 1% FBS. Allantoin at the same concentration was used as the positive control and the experiment was done in triplicates. The plate was viewed under a light microscope and images were taken at t₀, t₂₄, t₄₈, and t₇₂ using the 10X magnification. The images were analyzed using ImageJ (ij153-win-java8). The % wound closure was calculated using EQ 2.1

$$\text{EQ 2.1: \% Wound closure} = \frac{(\text{pre-migration}) - (\text{migration})}{\text{pre-migration}} \times 100\%$$

Where, ‘pre-migration’ is the initial area of the wound at t0 and ‘migration’ is the wound area after a particular time point (t24 – t72). After 72hrs, the cells were trypsinized and cell count was performed using Trypan blue dye exclusion.

2.6 Statistical analysis

The data are presented as means \pm standard deviation which were obtained from three independent experiments. The difference between the means was considered to be significant if $p < 0.05$ according to two-way ANOVA.



CHAPTER 3: RESULTS AND DISCUSSION

3.1 Synthesis and characterization of RW-AuNPs.

The AuNPs are some of the most expansively studied NPs amongst all noble metal NPs for the reason of their numerous surface functionalities and exceptional surface plasmon resonance that can be employed in many features. The making of AuNPs by green synthesis is meek and facetious. The NPs can be produced under a moderate environment without using elevated temperatures or pressures. The most common production method is the extracellular nanoparticle production method. The production is initiated by tetrachloroaurate salt. After mixing the metal salt and the measured red wine, the mixture is stirred on a thermo-shaker to produce the NPs. The color changed to a wine-red indicating the successful synthesis of the AuNPs. This is then followed by centrifugation and drying of the NPs for characterization and later usage. Differences in parameters and reaction environment have a significant impact on the physicochemical properties of AuNPs (such as their shape, size, and surface charge) which must be ideally controlled for their better applications such as scratch assay test for wound healing in this study.

3.1.1 Optimization of RW-AuNPs synthesis

Optimization of AuNP synthesis was conducted for the selection of effective synthesis parameters for the RW-AuNPs. In the search for optimal reaction conditions that favor a green synthesis approach and formation of stable AuNPs, five reaction parameters were optimized (Domany *et al.*, 2018);(Eskandari-nojehdehi *et al.*, 2016) these included the concentration of RW-Es, concentration of gold salt, temperature, pH, and incubation time. To achieve this, one parameter was varied at a time, and the others kept constant, and the progress of the reaction was monitored visually and by UV-Vis. The parameters for the synthesis of the RW-AuNPs were optimized resulting in mono-dispersed AuNPs with an average hydrodynamic size of 1-100nm and the PDI values at ≤ 0.5 . The colour changes from yellow to a brick-red or wine-red was a first indication of the presence of Au⁰ and that the AuNPs were synthesized (Alberti *et al.*, 2021) and this was further confirmed by the SPR at ~ 500 nm using the UV-Vis spectra (Santhoshkumar *et al.*, 2017).

- (i) Effect of temperature and concentration of RW-Es on the synthesis of RW-AuNPs

To investigate the optimum concentration of PN and P extracts on the synthesis of PN-AuNPs and P-AuNPs, 1mM gold salt was incubated at different temperatures with extract concentrations ranging from 1.56 - 50 mg/mL of PN-E and 3.125 - 100mg/mL of P-E while shaking at 1000rpm. The wine red colour developed at a slower rate for PN-AuNPs at lower concentrations (1.56 to 12,5mg/mL) than higher concentrations (50 and 100mg/mL) as shown in **Figure 3.1**. The colour intensity increased with increasing concentration with 100mg/mL reaching a blue-purple colour indicating NP aggregation (Allen *et al.* 2017). The complete bio-reduction reaction of AuNPs was indicated by the formation of a stable wine red colour (Boomi *et al.*, 2020). The reduction of the metal ion was further confirmed by the UV-Vis spectrophotometer. UV-Vis spectroscopy is a simple and essential analytical technique for the authentication of the AuNP formation and can give a rough estimation of the size, shape, and concentration of the AuNPs formed. The AuNPs absorb UV-visible light, then the absorbed radiation results in electron excitation from a low energy to high energy level (Pentassuglia *et al.*, 2018), and usually characterized by an SPR between 500nm and 580nm (Santhoshkumar *et al.*, 2017)

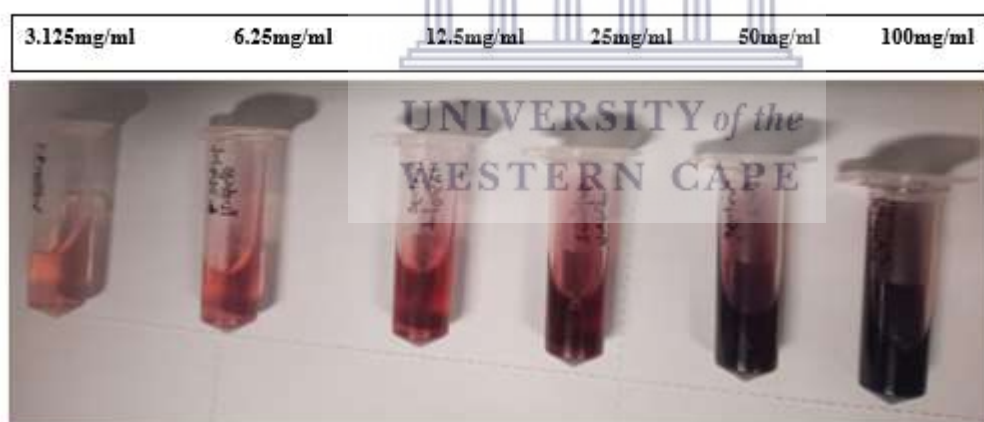


Figure 3.1: PN-AuNPs synthesized from different concentrations of PN-E and 1mM gold salt at 25°C.

The UV-Vis spectra of PN-AuNPs and P-AuNPs shown in **Figure 3.2** were recorded after 1hr incubation. Generally, the absorption peaks (SPR) varied significantly for the two extracts at different concentrations and temperatures. Lower concentrations of the extracts resulted in broad peaks and this may be due to the ratio of reducing agent to Au ions in the solution. The amount of reducing agents in the solution might have been insufficient hence fewer AuNPs were synthesized (Ngungeni, 2019). Increasing the concentration was expected to increase λ_{max} (SPR) and the amount of AuNPs formed. Although this is the case, very

high concentrations of the extract may lead to competition between the ions in the gold and those of the extract and this was observed as a decrease in the SPR for relatively high concentrations. Increasing the concentration of the extract resulted in the formation of large-sized and agglomerated NPs and this is due to the competition that occurred between the functional groups in the RW-Es and gold ions. Temperature played an important role in the synthesis of AuNPs in that, a higher rate of reaction was observed in higher temperatures. However, high temperatures require high inputs of energy, and this is unfavorable for a greener synthesis method. The lowest possible temperature for small-sized and mono-dispersed NPs is preferred for the green synthesis of NPs.



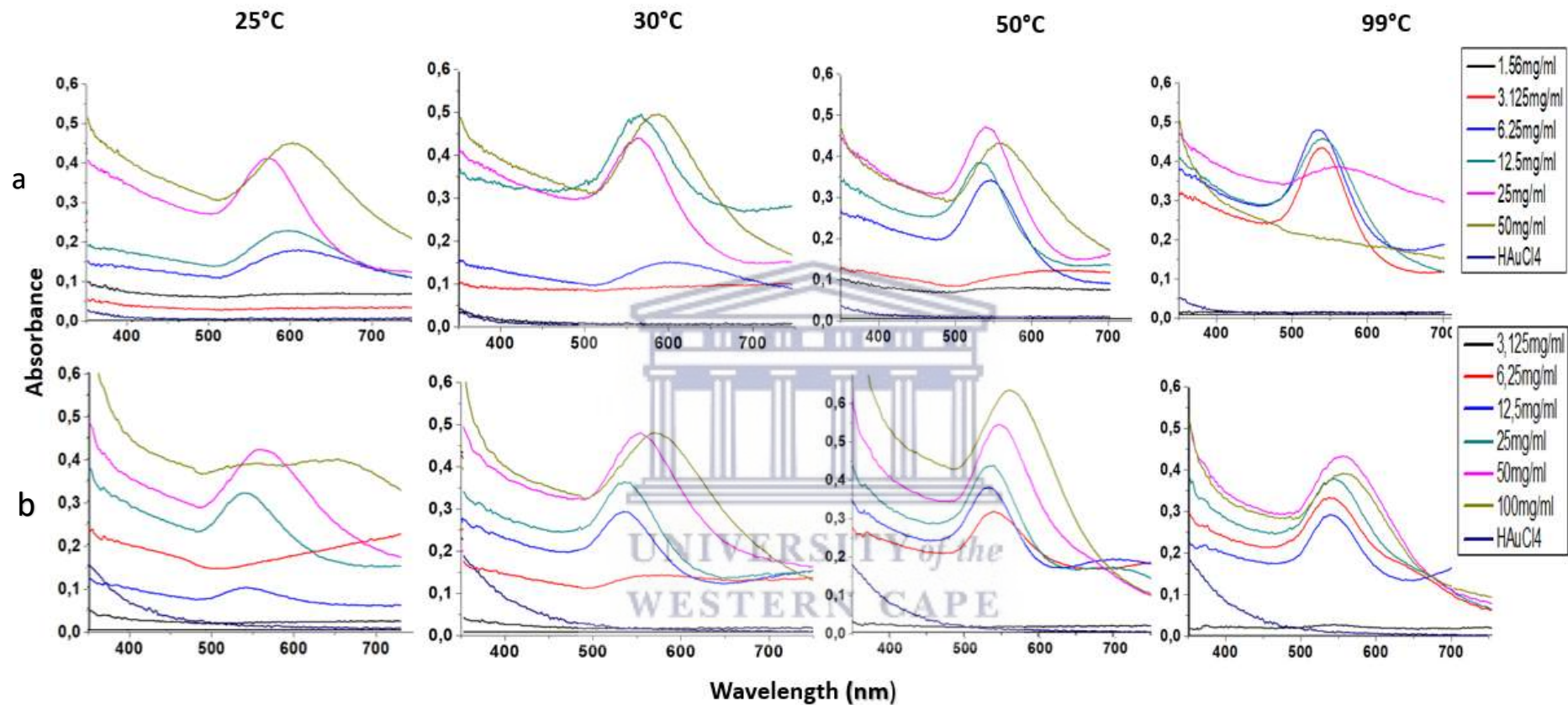


Figure 3.2 UV-Vis spectra of PN and P AuNPs. The AuNPs were synthesized at different temperatures 25°C, 50°C, 70°C and 99°C on a thermo-shaker operating at 1000rpm for 1hr at varying PN-E (a) and P-E (b) concentrations.

All temperatures allowed for the synthesis of PN-AuNPs as depicted by the formation of a peak around 550nm (**Figure 3.2 a**). At room temperature, only the concentrations $\geq 6.25\text{mg/mL}$ were able to synthesize PN-AuNPs. PN-E at 6.25mg/mL and 12.5mg/mL had broader peaks suggesting that the AuNPs were polydisperse. At lower temperatures, the amount of PN-AuNPs synthesized increased with increasing PN-E concentration (based on the absorbances at SPR). Between 25°C and 50°C, 1.56mg/mL and 3,12mg/mL of PN-E did not reduce or synthesize AuNPs and this was shown by the flat peaks. Surprisingly, at 99°C, the highest concentrations synthesized AuNPs with broader peaks. The PN-AuNPs formed by 25mg/mL of PN-E at 25°C appeared to be uniformly sized and was therefore selected as the optimum concentration and temperature for PN-AuNPs.

Similarly, all temperatures were able to synthesize P-AuNPs (**Figure 3.1 b**). Moreover, the lowest concentration of P-E did not favor the synthesis of P-AuNPs as indicated by lack of absorption peaks at 3.125mg/mL at all temperatures and 6.25mg/mL at 25 and 30°C. At room temperature (25°C), most of the peaks were broad at 25 and 50mg/mL with the λ_{max} at approximately 0.4 and 0.45 for 25 and 50mg/mL, respectively. At 50°C, 100 and 50mg/mL P-E formed AuNPs with narrower peaks compared to the lower concentrations suggesting that AuNPs were mono-dispersed and have a uniform size distribution at lower concentrations. There was a redshift between 50 and 100 mg/mL at 50°C. Increasing the temperature further to 70°C resulted in more AuNPs, quantitatively, from all the concentrations compared to lower temperatures. AuNP formation at all concentrations was symmetrical. The emerging peak around 760nm for 12,5 and 25 mg/mL suggested that AuNPs of different shapes were present. The RWE concentration was directly proportional to the amount of AuNPs. At 99°C, only 3.125mg/mL did not produce any AuNPs and 50mg/mL was selected as the optimal concentration at 50°C for P-AuNP synthesis. This temperature is moderate and therefore acceptable as a green synthesis. At 50°C, reactions are expected to have lesser reaction times. The reaction time for a study using 1mM gold salt in the synthesis of AuNPs from *Fenugreek* seed extracts was 10min (Daruich *et al.*, 2019).

(ii) Effect of concentration of gold salt on the synthesis of RW-AuNPs

The effect of gold salt concentration on the synthesis of the three RW-AuNPs at their optimal concentration and temperature was investigated at a range of 0.25 – 5 mM. The optimal conditions for CS-AuNPs were investigated in a previous study. 12.5mg/mL of CS-E was reacted with 1mM gold salt at 50°C on a thermoshaker operated at 1000rpm. A colour change

in a solution from yellow to wine-red was used as an indication that AuNPs have been successfully synthesized. As shown in **Figure 3.3**, it was visually evident that the only 1mM HAuCl₄ concentration was able to synthesize the PN-AuNPs. The results obtained prove that high metal salt concentrations increase the nucleation process, thereby producing larger NPs, and sometimes no NPs are produced. These results were similar for the P- and CS-AuNPs (data not shown). Studies have shown that 1mM gold salt was optimal for the synthesis of AuNPs (Elbagory *et al.*, 2016);(Vijayakumar *et al.*, 2017)



Figure 3.3. The effect of gold salt concentrations is the synthesis of RW-AuNPs. 0,25, 0,5, 0,75, 1, 2, 3, 4 and 5mM HAuCl₄ are used in the synthesis performed on a thermo-shaker operating at 1000rpm at optimized temperatures.

(iii) Effect of pH on RW-AuNPs synthesis

pH induces the reactivity of the extract with gold ions. Previous studies have shown that Au³⁺ can be reduced to Au⁰ in alkaline solutions (Sokolsky-Papkov & Kabanov, 2019) The reduction potential of polyphenols is dependent on the pH and decreases as the pH increases (Oueslati *et al.*, 2020). To study the effects of pH on the formation and stability of the RW-AuNPs; RW-Es of varying pH (3,5 – 10) were prepared and used in the synthesis at the optimal temperature and concentrations. The appearance of the visible wine red colour in **Figure 3.4** indicated that AuNPs were synthesized at all pH values. The intensity of the color of the AuNPs was directly proportional to the concentration of the AuNPs i.e the AuNPs had a light red colour at low pH to a darker red and purple colours with increasing pH for all the RW-Es indicating that more AuNPs were synthesized at higher pH.

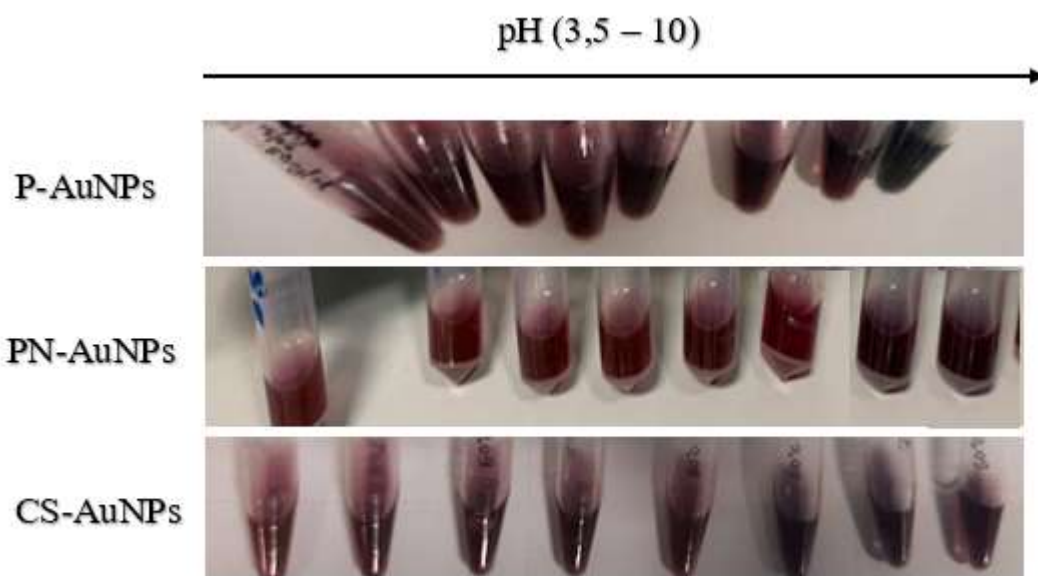


Figure 3.4: Effect of increasing RWE pH on the RW-AuNP synthesis.

To further investigate the effects of pH in the synthesis of RW-AuNPs, the SPR of the AuNPs were monitored by UV-Vis and shown in **Figure 3.5**. The RW-Es produced RW-AuNPs at all tested pH. The CS-AuNPs synthesized at pH 6 and pH 8 had two peaks (one around 550 and another around 800nm) suggesting differently shaped AuNPs in the solution compared to the other pH (**Figure 3.5 a**). pH 8 and pH 9 had similar UV-Vis profiles but pH 7 was slightly red-shifted. pH 4 was selected as the optimal pH for the synthesis of CS-AuNPs with uniform shapes. **Figure 3.5 b** represents the formation of P-AuNPs and the peaks show that increasing the pH of C-SE forms more AuNPs compared to biological pH (3.852). pH 10 had the broadest peak, an indication of polydisperse AuNP formation. pH 5 was selected for the synthesis of P-AuNPs as it formed a considerable amount of AuNPs with a desirable narrower peak. **Figure 3.5 c**, the spectra show that in all these pH levels, PN-AuNPs can be synthesized but with increasing pH (to more basic) resulted in polydisperse AuNPs. The spectra for pH 6 and 7 show narrow peaks which mean that the AuNPs formed are smaller in size and are monodispersed. pH 7 and 10 AuNPs precipitated out of the solution after an hr, hence pH 6 being was selected as the optimum pH.

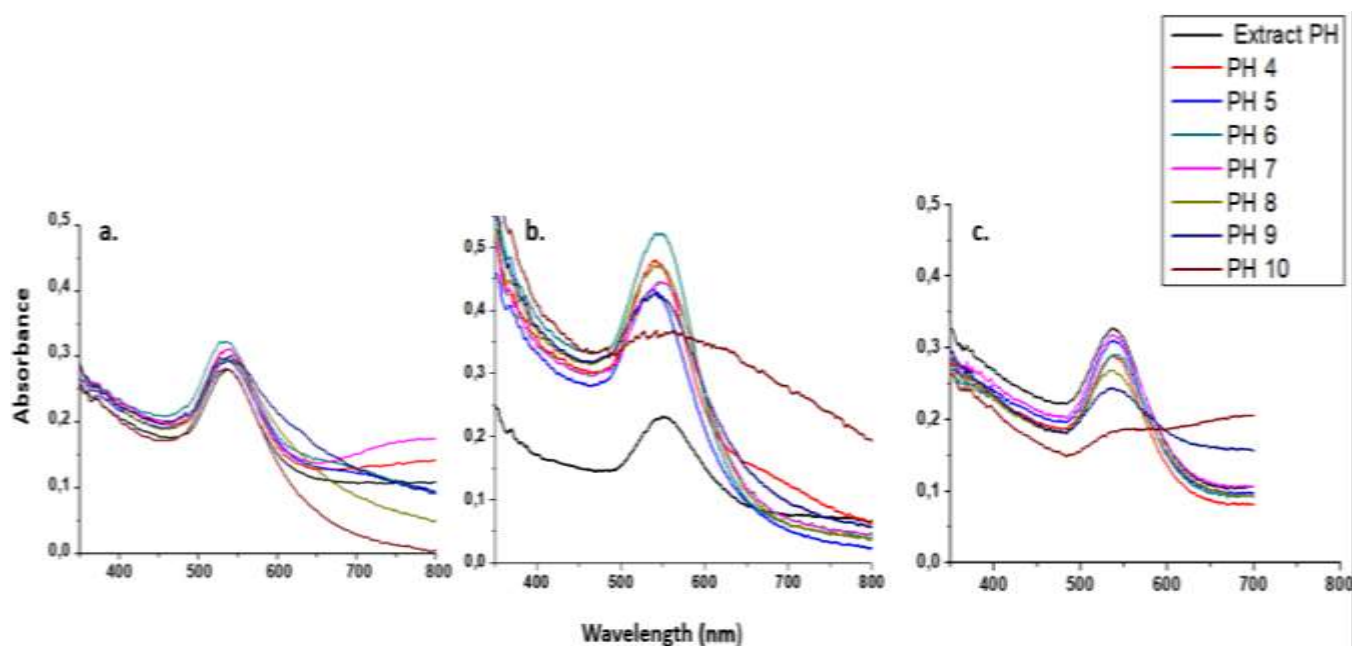


Figure 3.5: UV-Vis spectra of SPR bands representing AuNPs formed from (a) CS, (b) P and (PN) extracts at extract pH, pH 4, 5, 6, 7, 8, 9 and 10 using optimized concentrations and temperature.

3.1.2 Reaction Kinetics for synthesis of RW-AuNPs

The kinetics of RW-AuNP formation was studied by observing the changes in λ_{max} (SPR) in the UV-Vis spectra obtained from AuNPs synthesized throughout 240mins (4hrs). To evaluate the effects of time on the synthesis of AuNP reaction, the reaction was carried out at the aforementioned optimized reaction parameters and aliquots of the solution were taken periodically between 0 and 240min and monitored by UV-Vis in the range 350 and 700nm.

The UV-Vis spectra of all the AuNPs in **Figure 3.6** showed that as the reaction time increases, the absorbance increases meaning the amount of AuNPs in solution were increasing. The intensity of the peaks increased with time and became constant after 120min for P-AuNPs and CS-AuNPs, and at 150 min for PN-AuNPs. The plateau indicated completion of the reduction or reaction (Ahmad *et al.*, 2016). **Figure 3.6 a-c** shows the UV Vis spectra at different time points, whereas **Figure 3.6 d-f** shows the reaction rates of the RW-AuNPs. The rapid increase in absorbance for the first hour is attributed to the reduction of Au^{3+} to Au^0 and the increase in the amount of AuNPs. The CS- and P-AuNPs reached a maximum absorbance at 120min, 30 min before PN-AuNPs and this suggested that the phytochemicals in these extracts, may have higher reducing powers compared to PN-E. The λ_{max} for PN-AuNPs remained relatively constant between 50min and 120min but the peaks

were broad and became narrowed after 180 min of synthesis. It also should be noted that PN-E was used at a concentration that was 50% less than the CS-E and this may also lower the reaction rate (25mg/mL and 50mg/mL for PN-E and CS-E, respectively). The PN-E concentration might have affected their bioreduction activity and therefore the rate of reaction.



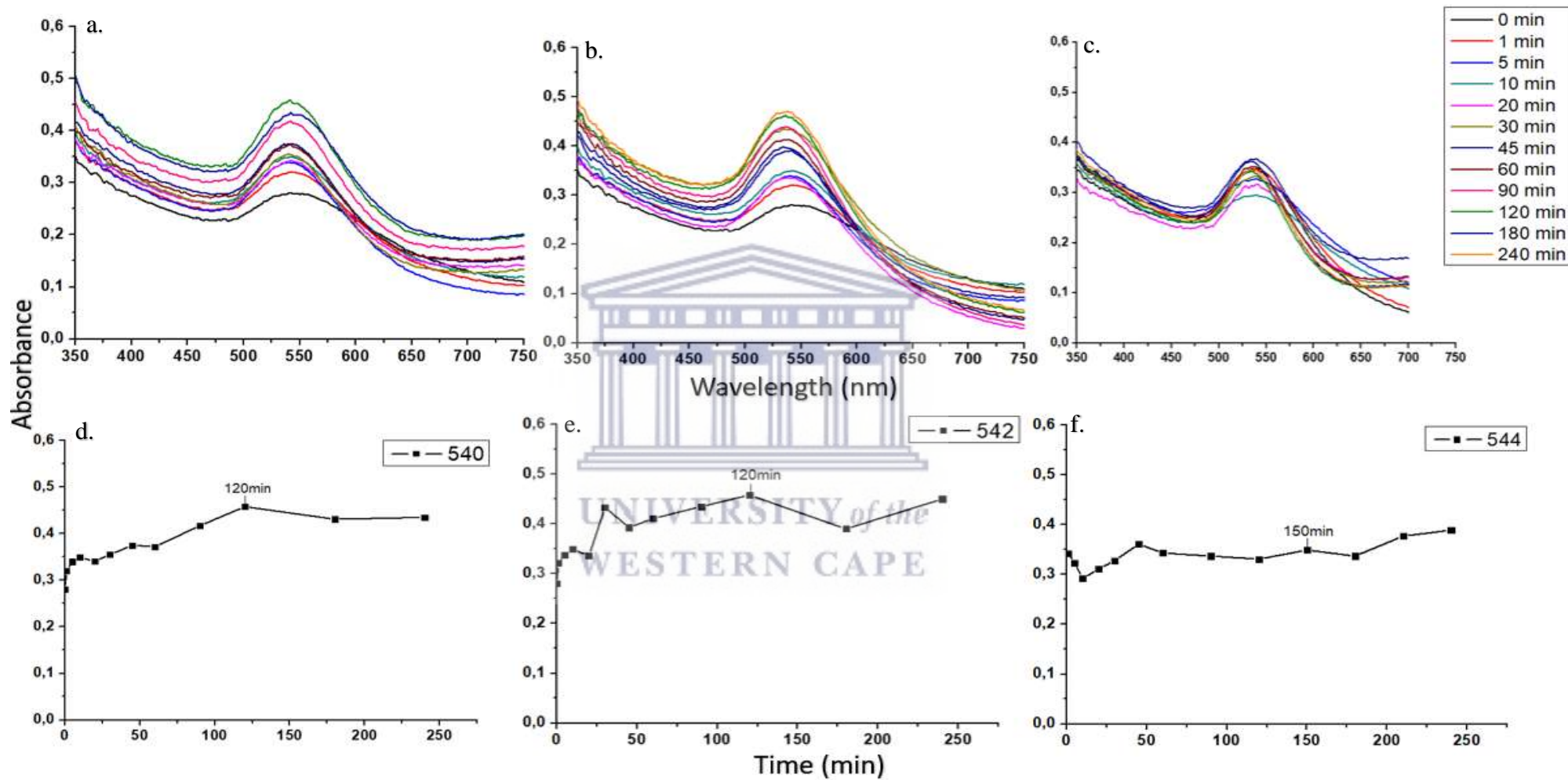


Figure 3.6: UV-Vis spectra recorded as a function of time for the synthesis of AuNPs using (a) CSRW, (b) PRW, and (c) PNRW extracts at optimized pH, temperature, and concentration of extracts. (d), (e) and (f) is the change in absorbance maxima recorded with time.

3.1.3 Biosynthesis of RW-AuNPs using optimal conditions

Biologically inspired synthesis of AuNPs is becoming popular with increasing environmental impact consciousness. Not only are these methods eco-friendly, but they are also cost-effective and a rapid form of MNP synthesis. AuNP synthesis is of particular interest as they are the most stable form of MNPs (Ahmed *et al.*, 2016). Various studies have reported the successful synthesis of AuNPs from different plant extracts such as *Dracocephalum kotschi* (Dorosti & Jamshidi, 2016) and *Elaise guineensis* (Ahmed *et al.*, 2016).

The optimal conditions for the biosynthesis of RW-AuNPs are summarized in **Table 3.1**. The PN-AuNPs were synthesized using a stock solution of 25mg/mL of PN-E at pH 6 at ambient (room) temperature. The CS-AuNPs were synthesized with a stock solution of 12,5mg/mL of CS-E at pH 4 at 50°C, the P-AuNPs were synthesized with a stock solution of 50mg/mL of P-E at pH 5 at 50°C. All the RW-AuNPs were synthesized using 1mM HAuCl₄ using a 1:10 ratio of HAuCl₄ to RW-Es, 1:6 for CS-AuNPs.

Table 3.1: Optimal conditions for RW-AuNP synthesis.

RW-Es	[RW-Es]	[HAuCl ₄]	The molar ratio of Au salt to RW-Es	Temperature	pH	Synthesis time
PN-E	25mg/mL	1mM	1:10	25°C	6	2.5hrs
P-E	50mg/mL	1mM	1:10	50°C	5	2hrs
CS-E	12,5mg/mL	1mM	1:6	50°C	4	2hrs

The schematic representation of the overall synthesis of RW-AuNPs is shown in **Figure 3.7**. The RW-Es were prepared by rotary evaporation of 500mL of each wine at 50°C. The resulting dark purple coloured paste was oven-dried and stock solutions of RW-Es were prepared using deionized water. The RW-Es were mixed with HAuCl₄ to produce RW-AuNPs using the optimal conditions (**Table 3.1**), the color of the reaction mixture turned to a wine-red color as an indication of the successful conversion of ionic Au³⁺ to Au⁰. The color change was due to the surface Plasmon vibration of the MNPs which lie in the visible region on the electromagnetic spectrum (Menon *et al.*, 2017).

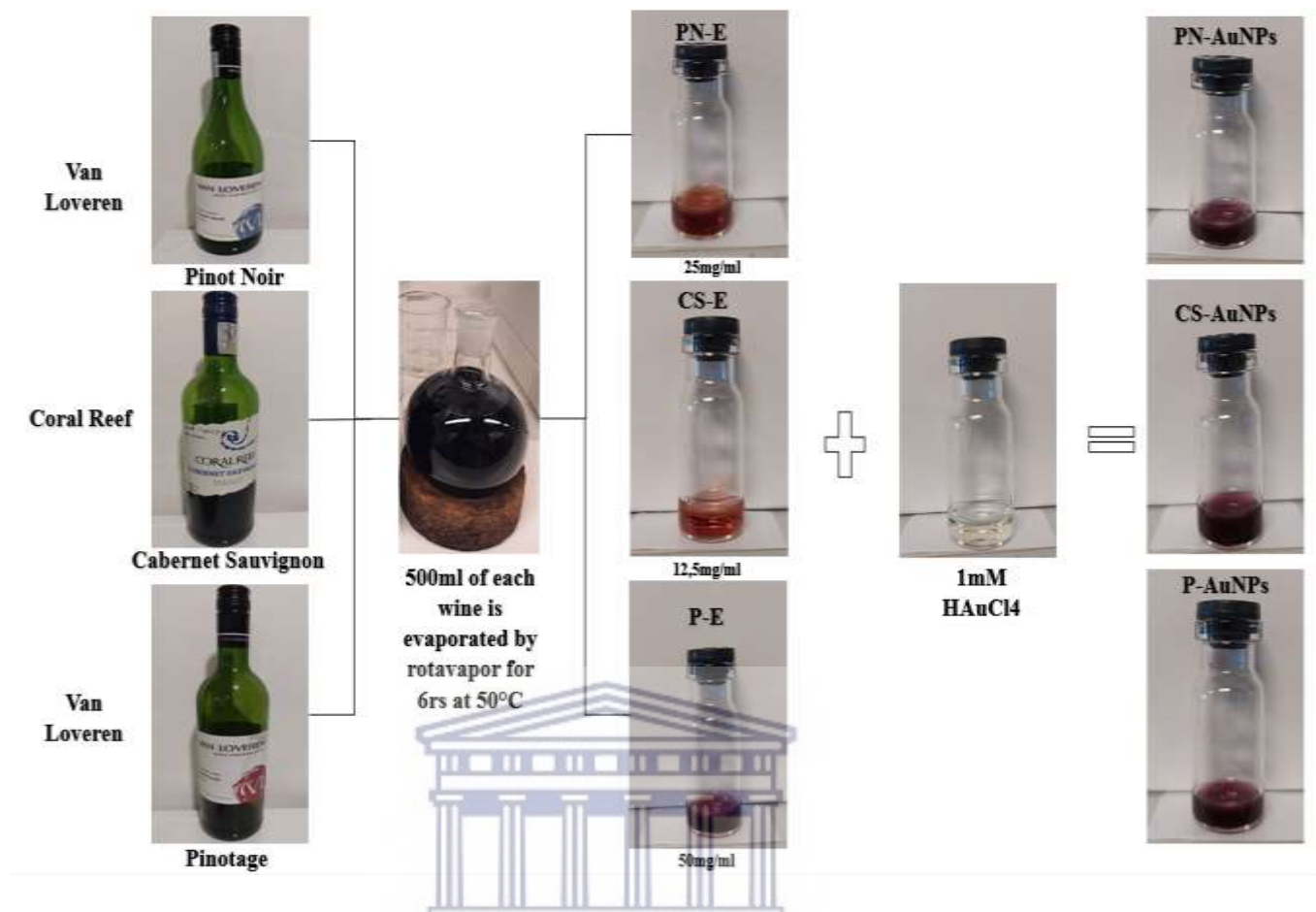


Figure 3.7: Schematic representation of the overall synthesis of AuNPs from RW-Es.

3.1.4 Optical properties of RW-AuNPs

The RW-AuNPs were analyzed by the UV-Vis following the colour change. The SPR provides information about the size, morphology, and relative concentration of the AuNPs. The SPR can also be influenced by the inter-particle distance, electron density, and the refractive index of the reaction medium (Rauh *et al.*, 2016). These factors can be tuned by altering the reaction parameters, not limited to the ones investigated in this study. A change in absorbance to a longer wavelength (the redshift) result from an increase in particle size and a reduction in particle size lead to a change in absorbance to a shorter wavelength or blue shift (Brause *et al.*, 2002).

Figure 3.8 shows the UV-Vis spectra of P-AuNPs, PN-AuNPs, and CS-AuNPs. For all the three RW-Es, the SPR band was obtained between 500 and 580 nm, which is characteristic of AuNPs (Haiss *et al.*, 2007). The λ_{max} for P-AuNPs, PN-AuNPs, and CS-AuNPs were 542nm, 544nm, and 540nm, respectively. The resulting peaks were symmetrical which means that the RW-AuNPs formed were of similar size and shapes. The band generated by P-AuNPs

was higher than CS-AuNPs, and lower than PN-AuNPs which suggested that more AuNPs were synthesized from PN-E followed by P-E. Two peaks were formed by P-E and similar results were previously obtained from the synthesis of AuNPs using 0.10 mol dm^{-3} 2-morpholinoethanesulfonic acid (MES) solution at pH 3.4, at this pH, the resulting UV-Vis spectra had two peaks (Habib *et al.*, 2005). The P-AuNPs had two absorption peaks, at 540 and 710 nm, the lower wavelength corresponding to transverse plasmon modes and the latter, longitudinal plasmon modes. The two peaks suggested a presence of non-spherical NPs (Philip, 2008), mostly rod-shaped AuNPs. The peak around 550nm is expected to have a lower absorbance compared to the one round 710nm. The dominant peak in the surface plasmon spectrum was along the transverse direction. This was an indication that, quantitatively, there are more nanospheres than nanorods (Shi *et al.*, 2012).

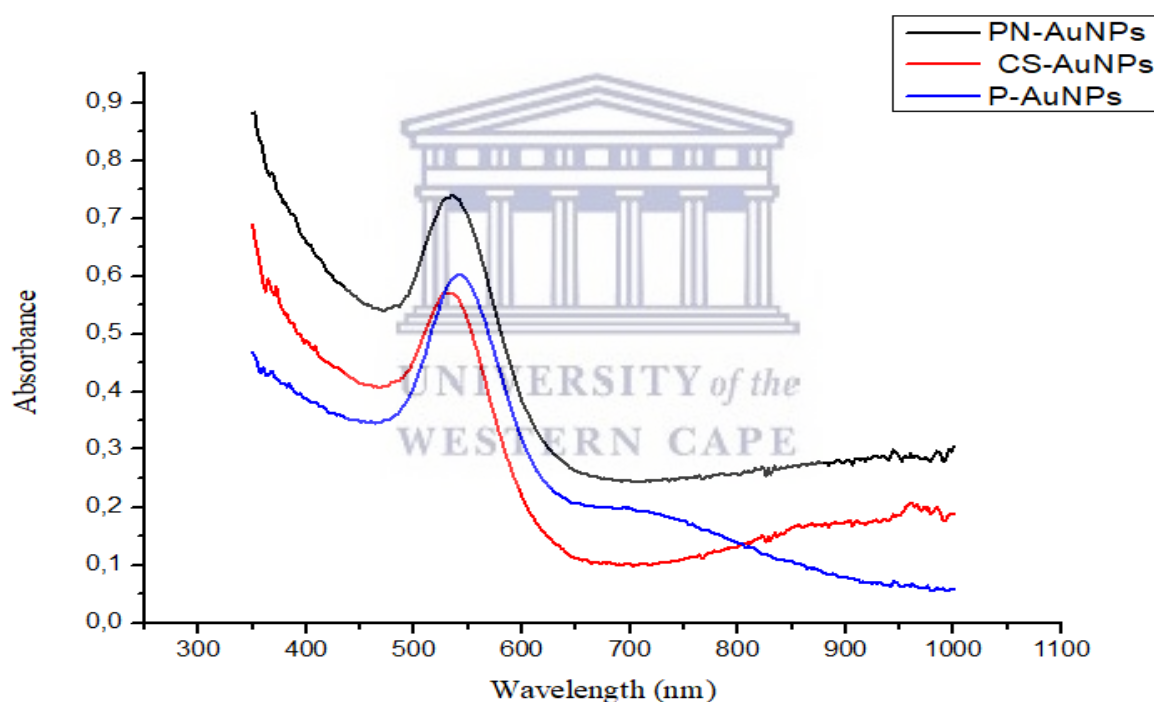


Figure 3.8: UV-Vis of PN-AuNPs, CS-AuNPs, and P-AuNPs synthesized at optimal reaction parameters.

3.1.5 DLS analysis

The resulting AuNPs were further confirmed by DLS analysis, to determine the hydrodynamic size, the PDI, and zeta potential. The hydrodynamic size accounts for the core size as well as the surface composition. PDI is the ratio of particles of different sizes to the total number of particles and ranges between 0 and 1. Polydispersed particles have higher

PDI (typically ≥ 0.7) and the PDI for monodispersed particles is lower (typically below 0.5) (Danaei *et al.*, 2018)

The size distribution versus intensity graph for CS, P, and PN-AuNPs synthesized at the optimum conditions is shown in **Figure 3.9**. The mean average hydrodynamic size for CS, P, and PN-AuNPs was 140.5nm, 98,7nm, and 85,87nm, respectively (**Table 4.2**). All the RW-AuNPs showed multimodal distribution, and the peak intensity was largely influenced by AuNPs with a hydrodynamic size ~ 100 nm (**Figure 3.9 a-c**). The CS-AuNPs had a larger hydrodynamic size compared to the other RW-AuNPs, and this may be due to the bio-organic molecules enveloping their cores (Prathna *et al.*, 2011). The PDI of the RW-AuNPs ranged between 0.2 and 0.5 (**Table 4.2**) affirming that RWE as stabilizing and reducing agents synthesized monodispersed and stable RW-AuNPs. The lowest PDI was obtained in CS-AuNPs (0.205) which suggested that the CS-E was able so to synthesize highly monodispersed AuNPs. Although PN-AuNPs had a relatively large PDI, they were still considered to be monodispersed.



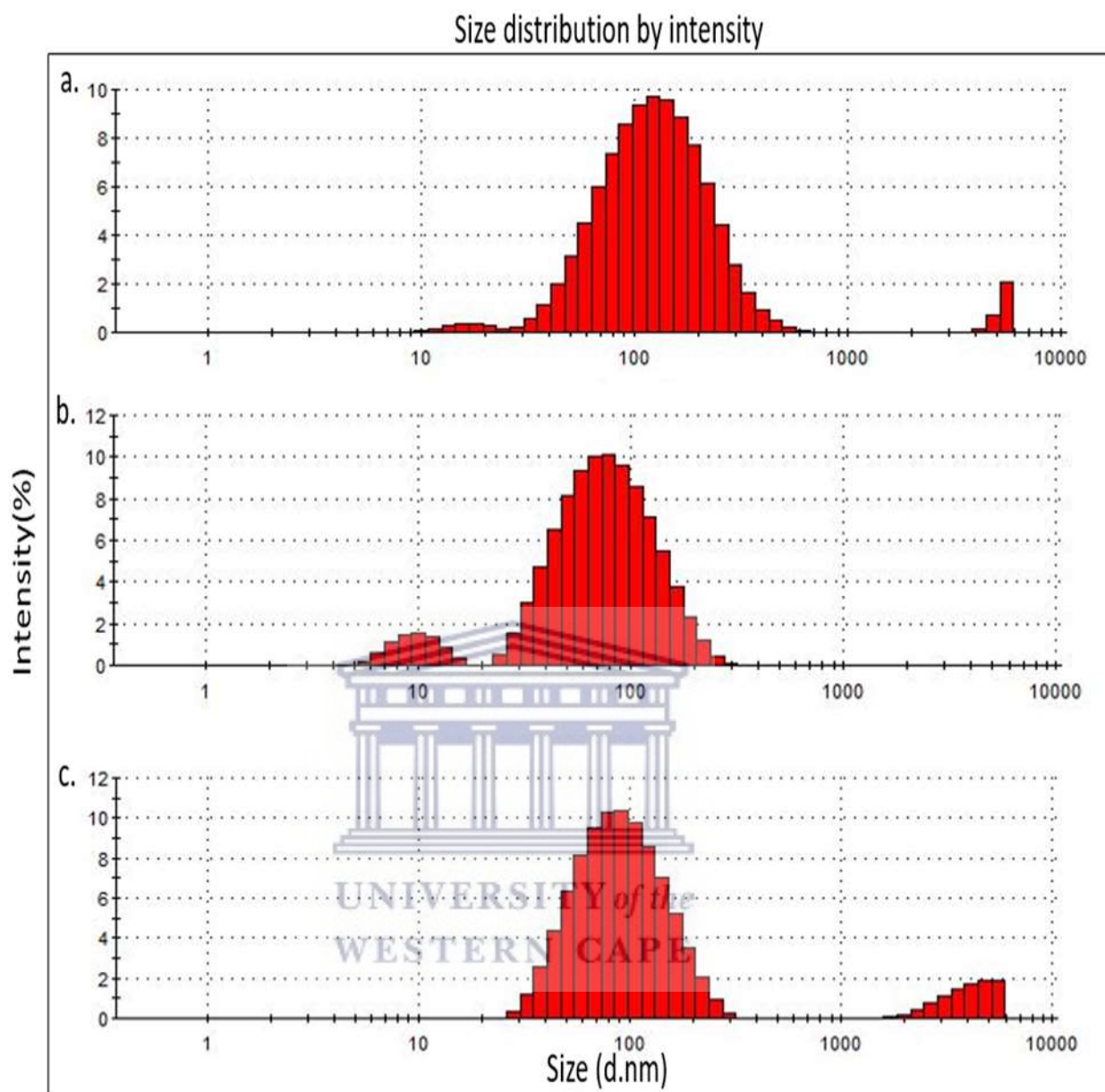


Figure 3.9 The hydrodynamic size distribution of CS (a), P (b) and PN (c) AuNPs synthesized at the optimal conditions.

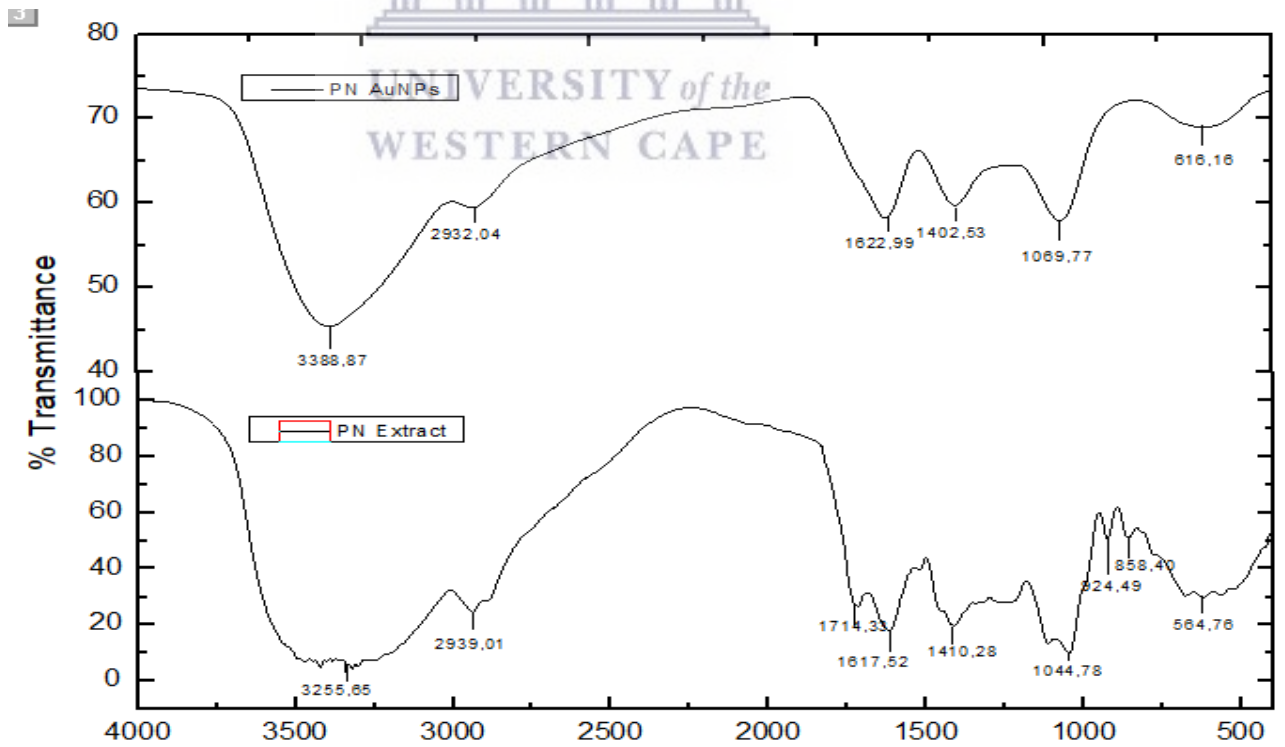
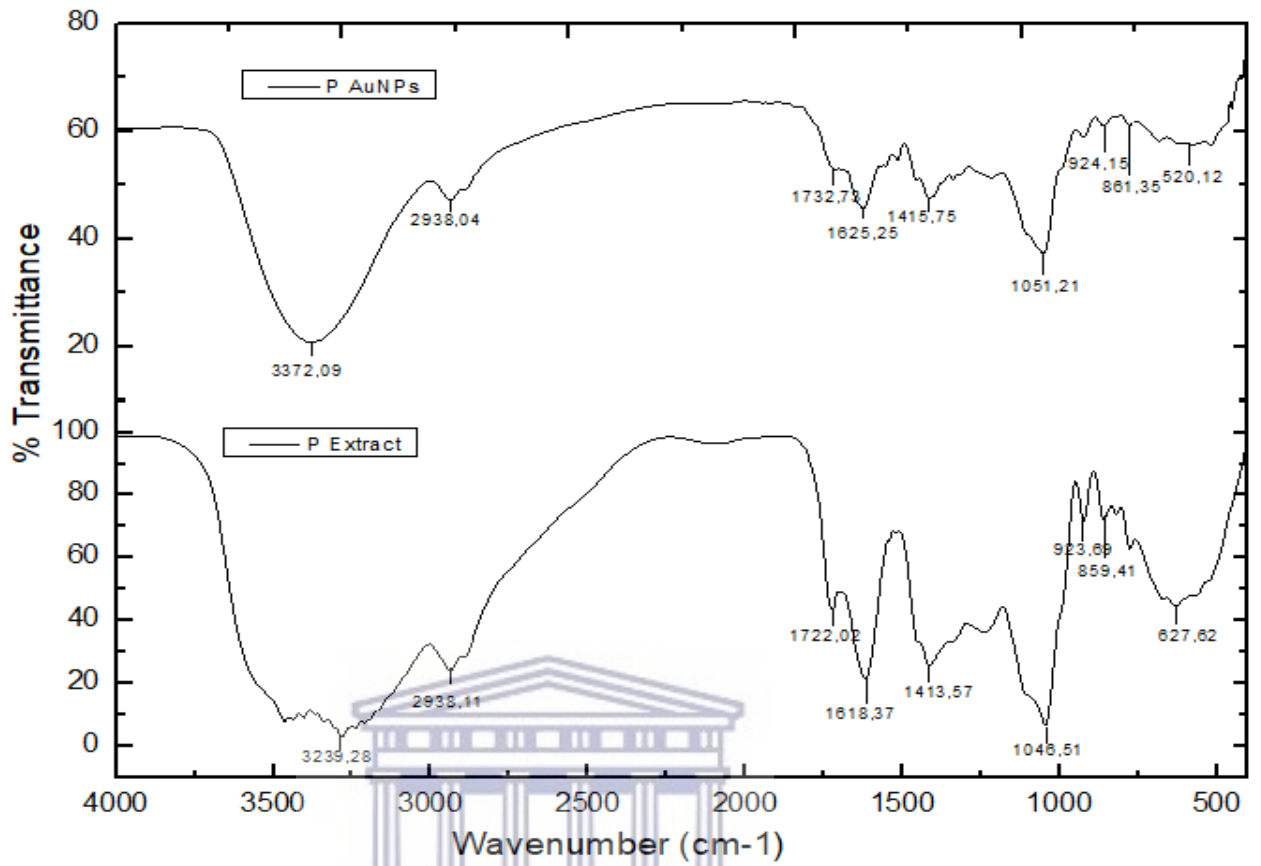
Table 3.2: Summary of the optical and DLS properties of the RW-AuNPs.

Sample	OC (mg/mL)	λ_{max}	Small particle size	Large particle size	Zavg	PDI
PN-AuNPs	25	544nm	2.27	82.13	51.60 ± 2.18	0.386 ± 0.04
CS-AuNPs	12.5	540nm	3.768	48.76	41.69 ± 3.69	0.205 ± 0.05
P-AuNPs	50	542nm	9.992	85.87	50.76 ± 1.74	0.444 ± 0.03

3.1.6 FT-IR analysis

The FT-IR analysis was performed on P-E, CS-E and PN-E and their corresponding AuNPs to determine which functional groups played a role in the reduction of Au^{3+} to Au^0 by comparing bands in the RW-Es and those present in the RW-AuNPs. The FT-IR identified several functional groups which were responsible for the biosynthesis of RW-AuNPs. The FT-IR spectra of the RW-Es and their respective AuNPs are shown in **Figure 3.10**. There are noticeable similarities between RW-Es and their corresponding AuNPs. Some of the peaks were transmitted at the same wavelengths and this suggested that some phytochemicals present in the RW-Es were also present on the surface of the RW-AuNPs. Some of the bands were shifted in AuNPs as compared to the extracts. The shifts are highlighted in **Table 3.3**.





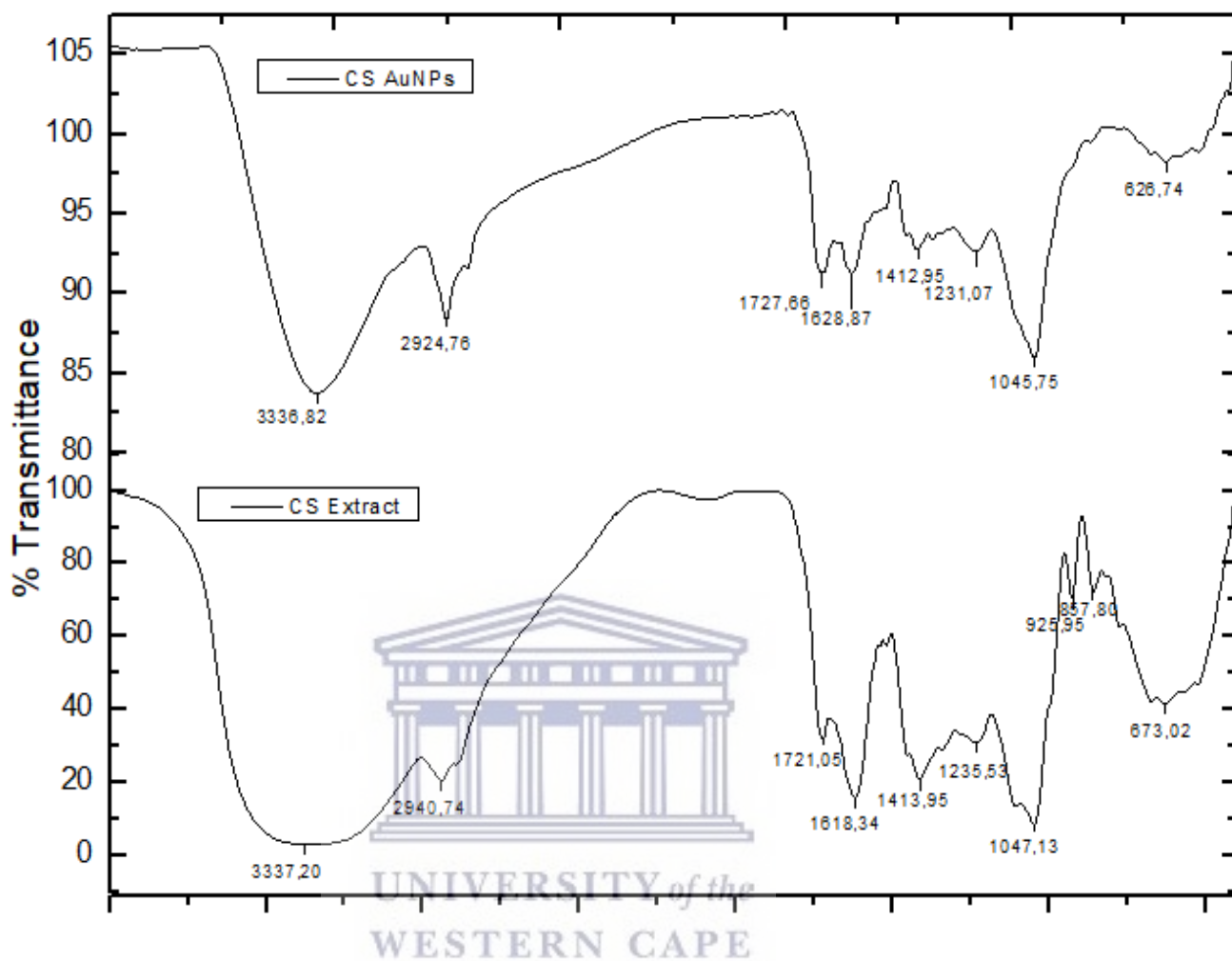


Figure 3.10 FT-IR spectra of RW-Es and the RW-AuNPs.

Table 3.3 Major peak shifts and their positions in the RW-Es as compared to their RW-AuNPs.

P			PN			CS			Possible functional group
band position in extract (cm ⁻¹)	band position in AuNPs (cm ⁻¹)	shift in position (cm ⁻¹)	band position in extract (cm ⁻¹)	band position in AuNPs (cm ⁻¹)	shift in position (cm ⁻¹)	band position in extract (cm ⁻¹)	band position in AuNPs (cm ⁻¹)	shift in position (cm ⁻¹)	
3239,28	3372,09	-132,81	3255,88	3388,87	-132,99	3337,2	3336,82	0,38	O-H (Alcohols and phenols)/ N-H (Amides)
2938,11	2938,09	0,02	2939,01	2932,04	6,97	2940,74	2924,76	15,98	C-H (Alkane)
1722,02	1732,7	-10,68				1721,05	1727,66	-6,61	C=O (ketones, carboxylic acids)
1618,37	1625,25	-6,88	1617,52	1622,99	-5,47	1618,34	1628,87	-10,53	Alkanes
1413,57	1415,75	-2,18	1410,25	1402,55	7,7	1413,95	1412,95	1	C-O / C-H (Carboxylic acids, Esters, Aromatic esters)
1045,51	1051,21	-5,7	1044,77	1064,78	-20,01	1047,13	1045,75	1,38	C-O-C
627,62	520,12	107,5	564,76	616,16	-51,4	673	626,74	46,26	C-Cl (alkyl halides)

Previous chemical studies have reported that RWs are rich in polyphenolic compounds such as tannins, anthocyanins, catechins and flavonoids, among others (Snopek *et al.*, 2018) and the transmittance of O-H and C-O in **Figure 3.10** and **Table 3.3** validates this. Numerous bands originating from wine phenols can be found in the 1680cm⁻¹ and 900cm⁻¹ region. The region in 1285cm⁻¹, in particular, is characteristic of flavonoid-based tannins (Edelmann *et al.*, 2001);(Fernandez & Agosin, 2007). The general observation from the FT-IR spectra of RW-AuNPs and RW-Es is the significant reduction in the broad O-H band between 3000cm⁻¹ and 4000cm⁻¹ for the extracts compared to the AuNPs. The extracts were not completely dry, but the AuNPs were completely dried, so the O-H is more prominent (Dorosti & Jamshidi, 2016). The C=O group identified between 1600 and 1400cm⁻¹ indicated the presence of carboxylic acids and was more defined in the extracts compared to the AuNPs. The extracts also contained polyphenols (evident in broad OH peak), this peak was smaller following synthesis, and this proves that the carboxylic polyphenols were responsible for reducing Au³⁺ to Au⁰. Studies have demonstrated that hydroxyls-containing compounds can act as reducing, stabilizing, and capping agents in the synthesis of AuNPs (Shankar *et al.*, 2014) . The bands around 700 to 900cm⁻¹ and 950 to 1285 cm⁻¹ respectively were attributed to the aromatic C-H out-of-plane and in-plane (Coates, 2006). The peak reductions and shifts were evidence of the biomolecule role in the synthesis of AuNPs. The presence of significant shifts around 1400cm⁻¹ suggested the involvement of esters, carboxylic acids, and aromatic esters in the bio-reduction of AuNPs (Dorosti & Jamshidi, 2016). It is expected that the significant peak shifts are noted around ~3300cm⁻¹, however, there are other noticeable changes throughout the spectra insulating the involvement of not only polyphenols but esters, carboxylic acids (Dorosti & Jamshidi, 2016) and amino acids (Balashanmugam *et al.*, 2016) in the synthesis of RW-AuNPs either as reducing and stabilizing agents (Veeraputhiran, 2013) .

3.2 Biological Assay

3.2.1 Determination of RW-AuNPs concentrations

The concentrations of P-, CS- and PN-AuNPs were determined by the ICP-OES, an analytical tool used to quantify the atomic/chemical composition of samples. The technique uses unique photophysical signals of each element to detect the amount of each element in a complex mixture (Levine, 2021). The gold content in the P-, CS- and PN-AuNPs was 202.14 $\mu\text{g/mL}$, 232.19 $\mu\text{g/mL}$, and 356.69 $\mu\text{g/mL}$, respectively.

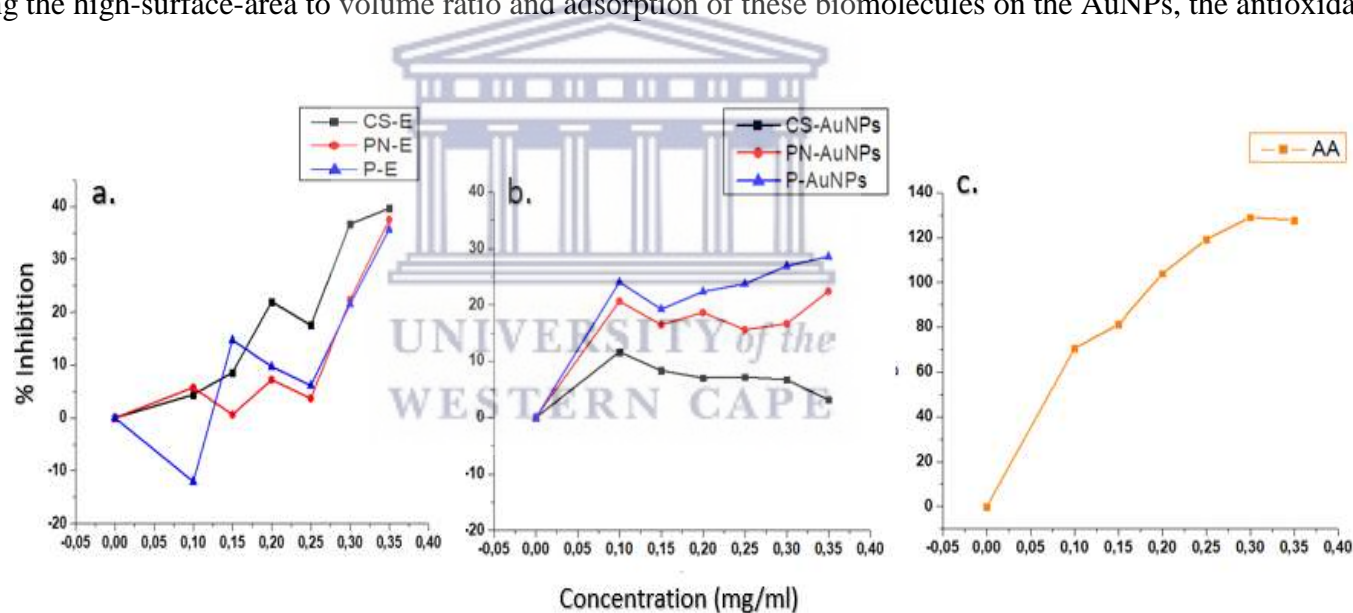
3.2.2 *In vitro* antioxidant activity

The use of plant extracts with antioxidant activities in wound treatment has increased dramatically over the years. In wound healing, antioxidant compounds enhance the healing of wounds by reducing the free radicals on the wound and this accelerates the wound healing process (Comino-Sanz *et al.*, 2021). DPPH free radical scavenging assay is a discoloration assay used to monitor the antioxidant activity of samples. The samples react with the stable DPPH and it is reduced and the color change from violet to yellow indicates the scavenging potential of an antioxidant agent (Akar *et al.*, 2017).

To evaluate the antioxidant activity of the RW-Es and RW-AuNPs, their reaction with DPPH as described in **section 2.3.7** was monitored by UV-Vis at 517nm. The DDPH assay has been utilized to evaluate the capability of AuNPs to perform as radical scavengers because DDPH radicals readily accept H^+ or e^- from compounds to neutralize themselves and the discoloration resulting from this reaction can be quantitatively measured from the changes in absorbance by UV-Vis. When DPPH is added to the samples with antioxidant ability, the colour changes from purple to yellow. The colour change indicates that these samples can transfer an H^+ or e^- to DPPH and converts it to DPPH-H (Ahn *et al.*, 2018).

Figure 4.1 showed that with increasing concentration, the radical scavenging ability of the RW AuNPs and the extracts increased, and this shows a dose-dependent radical scavenging activity. After the 30min incubation with the DPPH reagent, the IC_{50} of ascorbic acid (AA) was

calculated as 0.081mg/mL. In the tested concentrations (0.10 to 0.35mg/mL range) of the RW samples, the IC₅₀ of both the RW extracts and the AuNPs could not be determined. However, the RW-Es showed higher antioxidant activity compared to the AuNPs. The antioxidant activity and the phenolic content of wines have been reported (Di Majo *et al.*, 2008);(Stratil *et al.*,2008) and the RWs were reported to have a higher phenolic content compared to white wines. Interestingly, RWs with high polyphenolic contents tend to have a lower antioxidant activity as compared to those that have low polyphenolic content (Di Majo *et al.*, 2008). The antioxidant activity of the RW-AuNPs can therefore be attributed to the polyphenolic compounds of the RW-Es that tend to coat the AuNPs. The antioxidant activity of the RW-AuNPs at this concentration range was satisfactory but considering the high-surface-area to volume ratio and adsorption of these biomolecules on the AuNPs, the antioxidant activity



was expected to be higher.

Figure 4.1 Investigation of the antioxidant activity of RW extracts and AuNPs in relation to ascorbic acid using DPPH assay. a) %Inhibition for RW-E, b) RW-AuNPs and c) AA used as a standard.

3.2.3 *In vitro* stability testing of AuNPs

In order for AuNPs to be considered for biological applications, they need to maintain stability in different media. The stability of NPs can be greatly affected by interactions with biological media due to the high ion content and the presence of proteins in the biological fluid; all these can alter the chemical composition, surface chemistry, and colloidal properties of the NPs (Cedervall *et al.*, 2007). The biological environment is very complex, and interaction of the NPs with biological components can result in NP aggregation forming large and irregular-shaped NPs (Meakin, 1984). This phenomenon may alter the physicochemical properties, reactivity, bioavailability, and uptake of the NPs (Zhang, 2014), and consequently bystander effects.

The stability of the AuNPs was evaluated in water, complete DMEM, FBS, and PBS and monitored by the UV Vis spectra hourly for the first 6hrs and after 24hrs of incubation at 37°C. When the AuNPs aggregate and precipitate out of solution, their UV-Vis peak broadens, and a redshift is observed. The general observation with the RW-AuNPs is that there were no significant changes in the UV-Vis spectra of all AuNPs over a period of 24hrs (**Figure 4.2**) which suggested that the AuNPs remained in solution with no significant changes and are therefore stable in the test solution. Therefore, the RW-AuNPs can be used in a solutions that have high salt content (e.g PBS) or in the presence of the high abundant proteins in biological milieu (e.g albumin). Unstable AuNPs usually aggregate in the presence of salt (Pamies *et al.*, 2014) further confirming that the RW-AuNPs are stabilized by the RW phytochemicals.

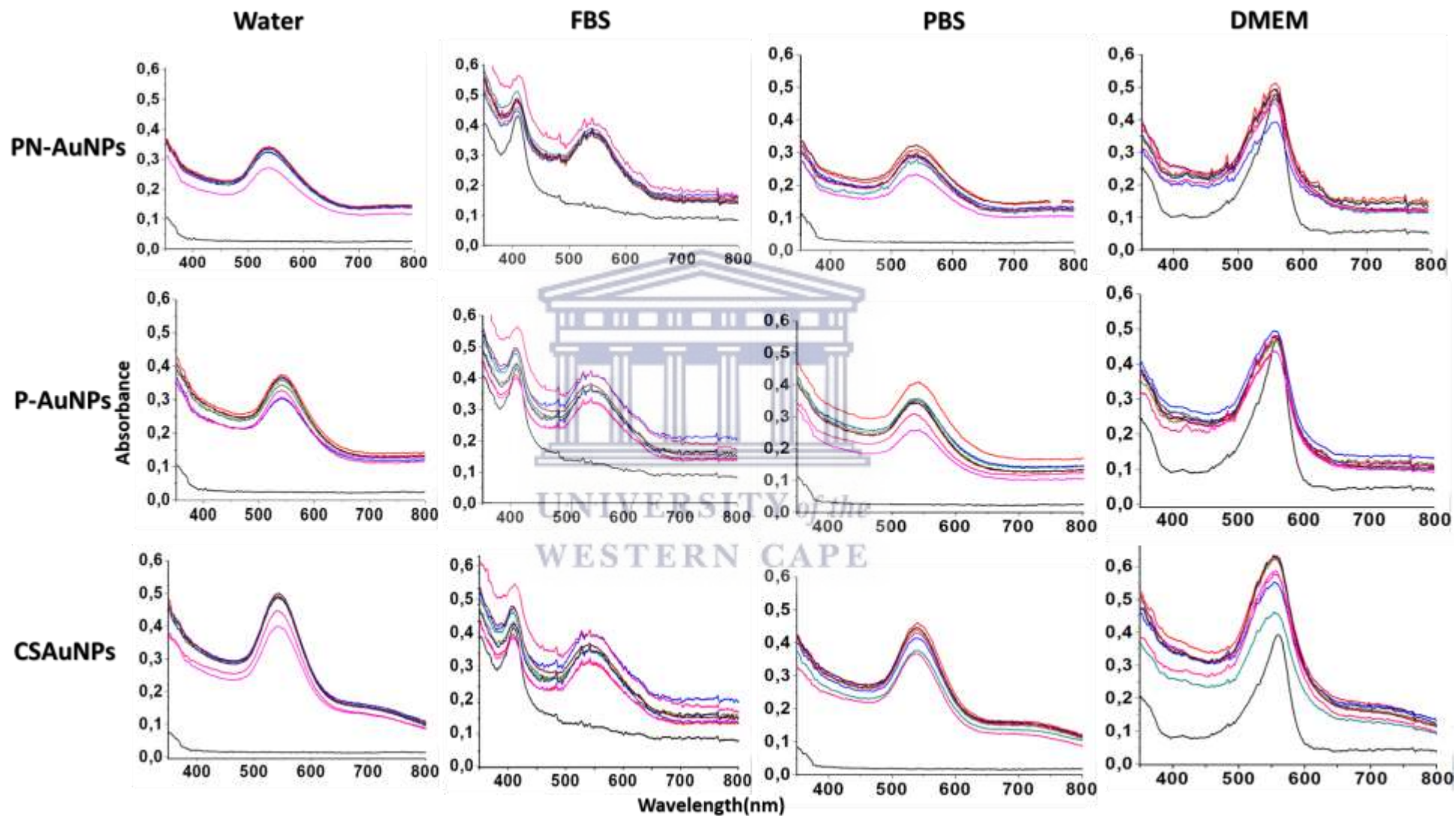


Figure 4.2: *In vitro* stability of RW-AuNPs during incubation at 37°C in solution. UV-Vis spectra spectra were taken periodically for 24hrs.

3.2.4 Evaluation of the wound healing effects of RW-AuNPs

AuNPs have great potential in biomedical applications such as drug delivery, imaging, and therapeutic agents (Nicole Remaliah Samantha Sibuyi *et al.*, 2021). However, there is limited information about the impact they may have on human health, for long- and short-term applications. Unlike their bulk counterparts, NPs possess unique physicochemical properties which allow them to penetrate and accumulate in the cells (Sani *et al.*, 2021) and therefore, their toxicity on cells ought to be evaluated before clinical application. This study aimed to explore the wound healing properties of RW-AuNPs on skin fibroblast (KMST-6) cell lines. The effect of RW-AuNPs on the viability of cells was determined by the MTT assay which is a quantitative assay based on the mitochondrial activity of viable cells. Viable cells can reduce the yellow tetrazolium salt into a purple compound that can be quantified by UV-Vis at 600 nm. The color intensity is directly proportional to the number of viable cells (Mosmann, 1983).

The effects of PN, P, and CS extracts and their corresponding AuNPs were tested on KMST-6 after 24hrs exposure following the procedure described in **section 2.3.8**. The cells were treated with increasing concentrations (0 to 1mg/mL) of RW-Es and (1.5625-50µg/mL) RW-AuNPs. The cell viability was assessed by MTT assay and represented as the percentage cell viability in relation to untreated cells.

(i) Effect of RW-Es and RW-AuNPs on KMST cells

The RW-Es and RW-AuNPs were not cytotoxic to the cells after 24hr treatment as shown in **Figure 4.3**. The viability for KMST-6 cells treated with RW-Es was unaffected by the extracts, except for P-E at the highest concentration which was reduced to 95% (**Figure 4.3 a**). The RW-AuNPs showed a noticeable increase in cell viability as the concentration of RW-AuNPs increases (**Figure 4.3 b**). The highest concentration (50µg/mL) reached astounding viability of above ~110% for the CS-AuNPs, and 120% for PN-AuNPs. The absence of any noticeable toxicity on the cells demonstrated a potential use of the RW-AuNPs in biological applications such as drug delivery, therapy, and wound healing.

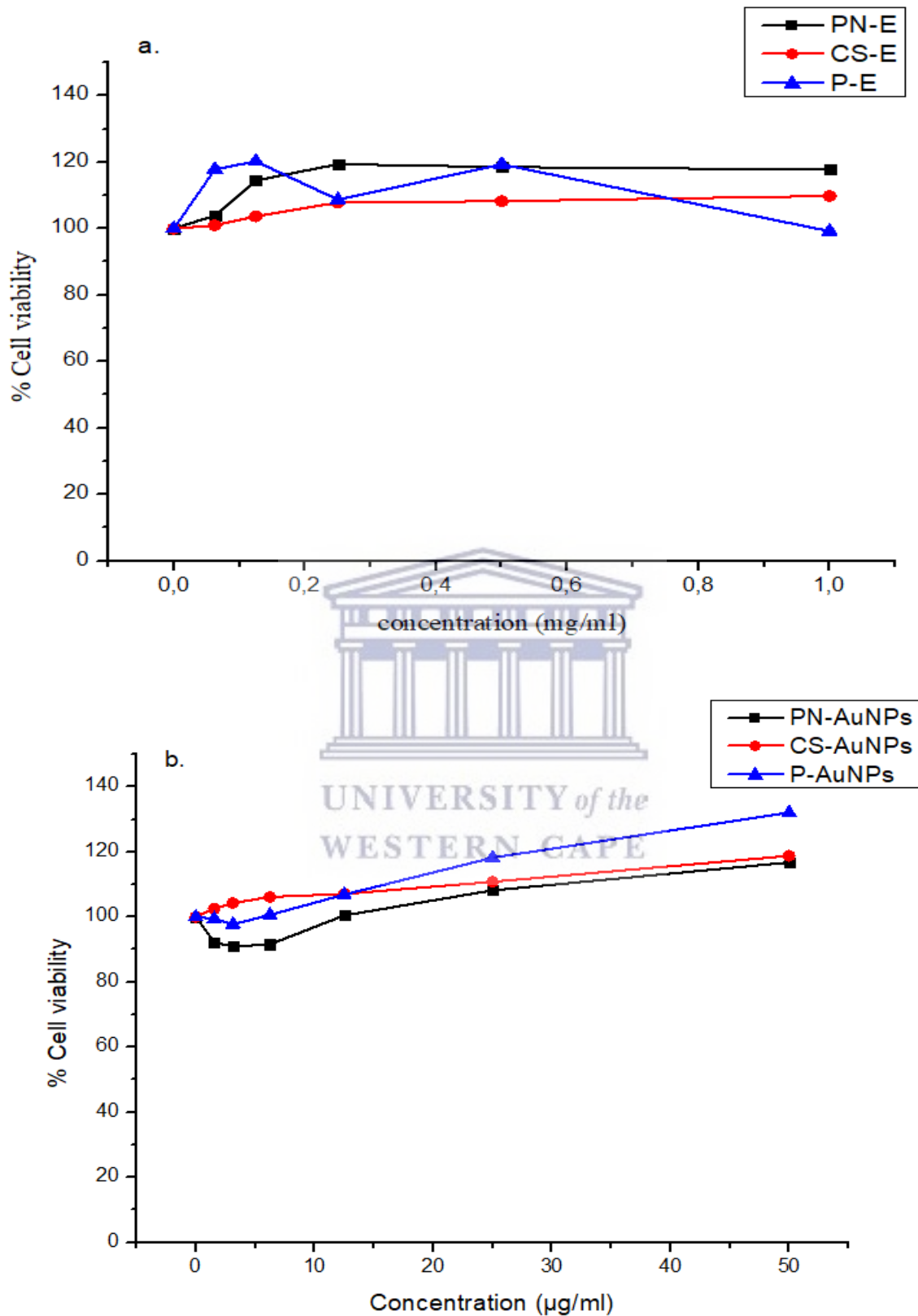


Figure 4.3. Effect of RW-Es and RW-AuNPs on KMST-6 cells. The cells were treated with increasing concentrations of RW-Es (a) ranging between 0.005 - 1mg/mL and RW-AuNPs (b) at 1.5625 - 50µg/mL for 24hr and cell viability was measured by MTT assay.

(ii) Effects of RW-AuNPs on cell migration

The ability of the RW-AuNPs to promote wound closure and healing was investigated by a scratch assay, an inexpensive and simple *in vitro* wound healing 2D technique (Kim *et al.*, 2020). Although the argument of whether this technique can be equated to actual wounds exists, this technique can be performed in a well-defined environment and has been successful in the investigation of cell migration properties of various compounds (Bowler *et al.*, 2001). In this technique, a scratch is made across a confluent cell monolayer and the migration of cells was monitored over time using the EVOS XL core light microscope. The scratch assay was performed on KMST-6 cells according to **section 2.3.9** and the images on the scratch were taken at different time intervals. The scratch or wound area was measured using the ImageJ software and this area was used to calculate the change in wound area.

The images in **Figure 4.4** illustrate how the wound gap changed over 72hrs in response to treatments. After 72hrs treatment, 100% of the wound gaps were closed for all samples except the PN-AuNPs. The cells treated with Allantoin, CS, and P AuNPs appeared to have overgrown after 72hrs when compared to the untreated cells. The overall wound closure for the CS-AuNPs and P-AuNPs was faster than that of the untreated cells. After the 48hr exposure, the wound closure for P-AuNPs and Allantoin had already reached an astounding 80%. In contrast, the wound gap on cells exposed to PN-AuNPs did not close after 72hrs. Of the three RW-AuNPs, the P-AuNPs followed by CS-AuNPs had comparable effects to Allantoin indicating their potential wound healing effects.

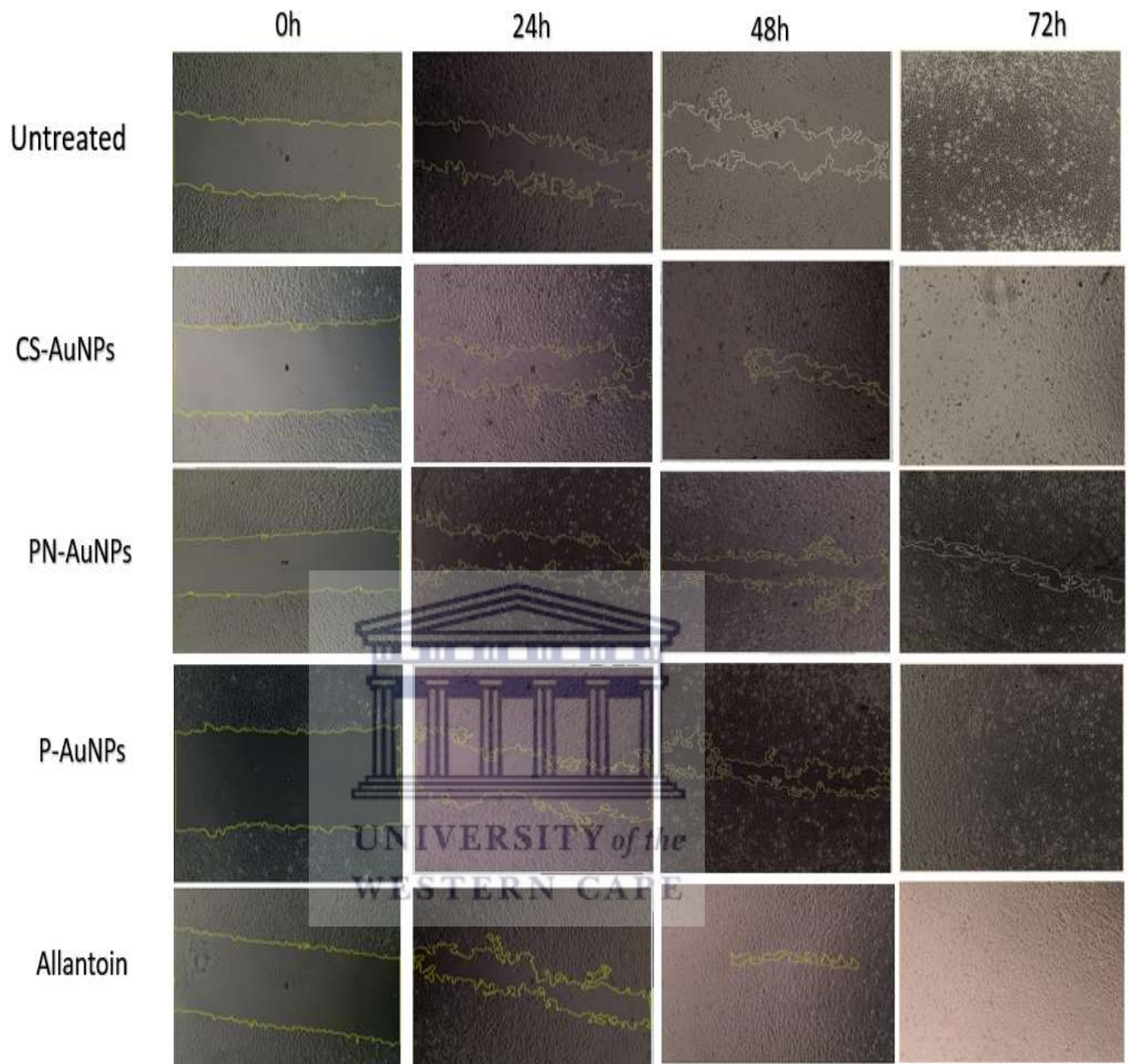


Figure 4.4 Effect of RW-AuNPs on KMST cell migration using a scratch assay. Scratch images were taken at 0h 24h, 48h and 72h after treatment with CS-AuNPs, PN-AuNPs and P-AuNPs and Allantoin as a positive control.

To determine the trend and the rate of wound closure, the area of the wound (in pixels) from each treatment was plotted against time as shown in **Figure 4.5**. There was a linear relationship between gap closure time and gap area, and the 2D continuum model of collective cell migration used by (Arciero *et al.*, 2013) predicts this behaviour. The first 48hrs of treatments resulted in the highest rate of wound closure, as indicated by the gradient of the slope. The positive control (Allantoin) has the steepest slope in the first 48hrs which suggests that it had the highest wound closure rate compared to the other treatments. Interestingly, the

rate of wound closure for the untreated and CS-AuNPs is slower in the following 24hrs compared to the other treatments. In the last 24hrs of treatment, the rate of wound closure decreased significantly. The images shown in **Figure 4.4** suggested that, during this period, cells die and this may result in a low to no wound closure.

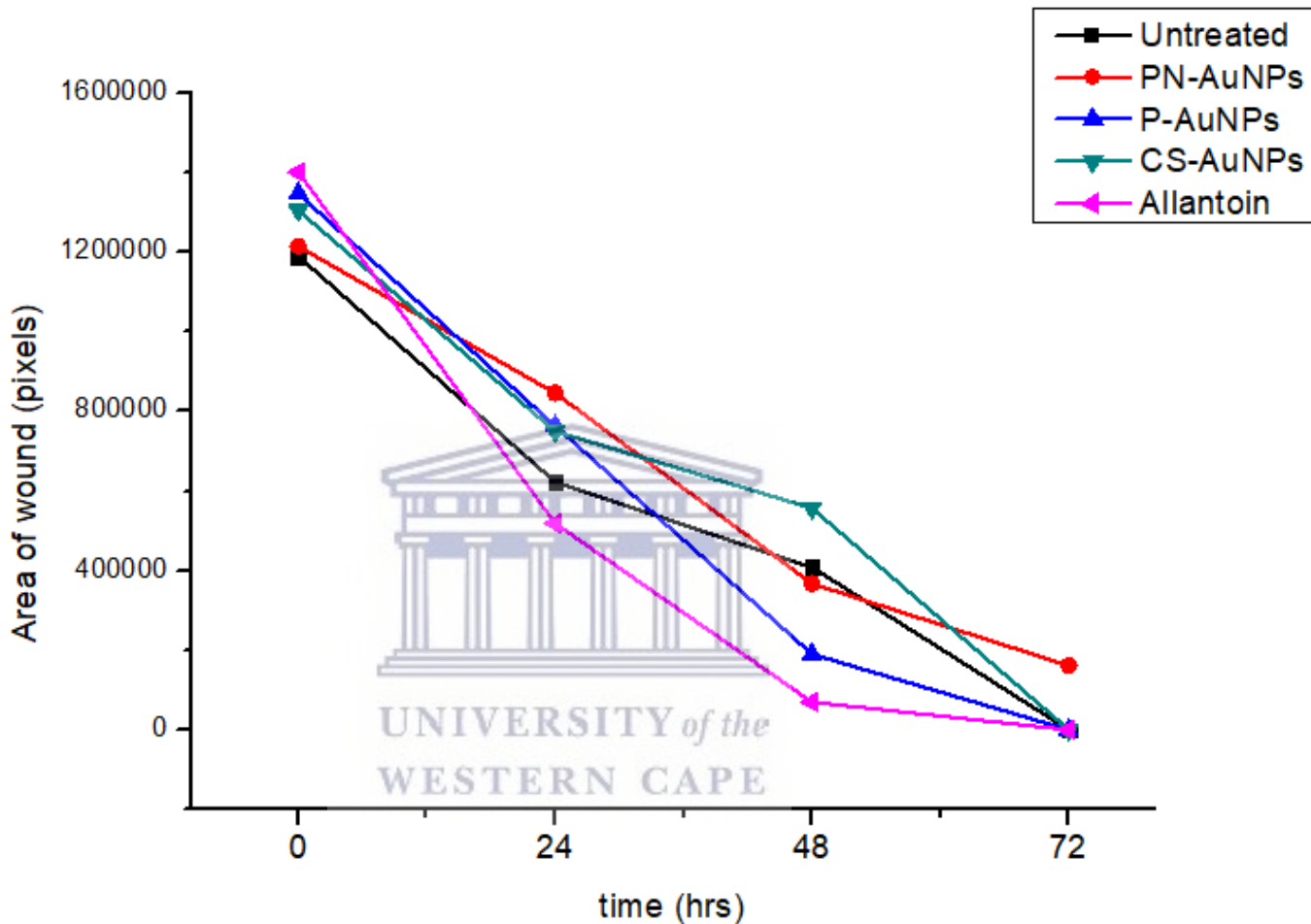


Figure 4.5 Change in area of wound gap (in pixels) over time after treatment with the RW (CS, PN, P) AuNPs. Untreated cells and Allantoin were used as the negative and positive controls, respectively.

Figure 4.6 shows the % wound closure calculated from the area of scratch using ImageJ. For the first 24hrs, Allantoin showed the highest wound closure with 50% of the wound closed after the 24hrs. The PN-AuNPs showed the least amount of wound closure in the first 24hrs, which unexpectedly exceeded the migration rate of cells treated with CS-AuNPs, P-AuNPs, and the untreated. After 72hrs, all treatments showed complete wound closure, except for the PN-AuNPs which showed 87% wound closure.

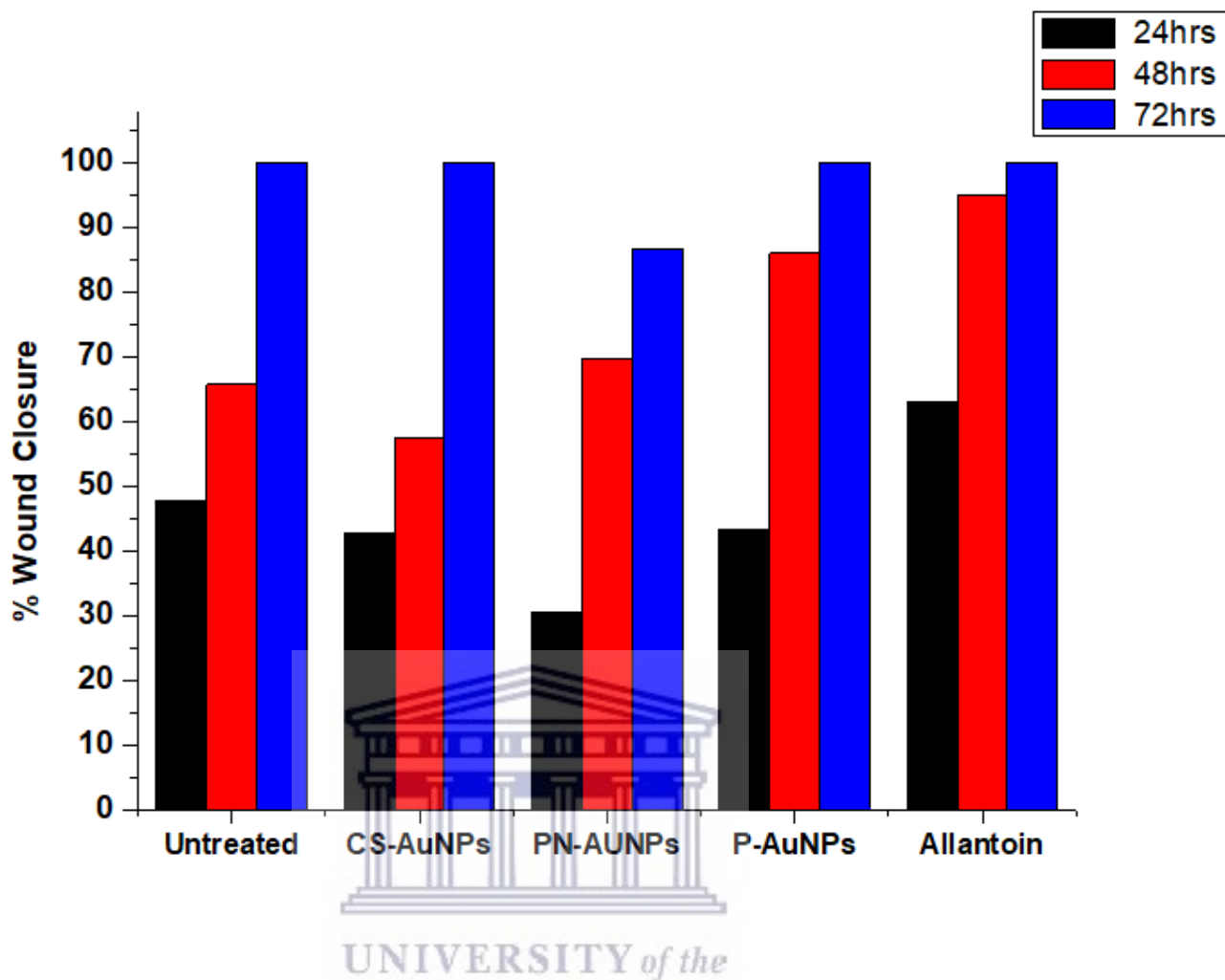


Figure 4.6. Wound closure (%) for KMST-6 cells. Untreated cells were used as a negative control and allantoin as a positive control. The closure was compared to cells treated with CS-AuNPs, PN-AuNPs, and P-AuNPs.

The number of cells in each well after the 72hr incubation was counted using Trypan Blue exclusion assay and the number of viable cells is shown in **Table 4.4**. Allantoin has been explored as a growth enhancer on HaCaT cells, the study showed that allantoin at 1, 5, and 10 μ g/mL promote cell proliferation and that genstisic acid however, had better effects (Kim *et al.*, 2020). In the current study, allantoin had the highest number of viable cells after 72hrs and was followed by P-AuNPs with a percentage cell viability of 110% (compared to the cell density at t=0hr). For a treatment to be considered a growth enhancer, the number of cells must be more than that of the untreated. The CS and P AuNPs can be considered as the growth enhancers, while PN-AuNPs on the other hand, suppressed cell growth.

Table 4.1: Cell density before and after treatment with RW-AuNPs

Treatment	t0 (cell/mL)	t72 (cell/mL)	% Increase in number of cells*
Untreated	2×10^5	3.72×10^5	86%
CS-AuNPs	2×10^5	3.84×10^5	92%
P-AuNPs	2×10^5	4.2×10^5	110%
PN-AuNPs	2×10^5	2.36×10^5	18%
Allantoin (pos)	2×10^5	5.6×10^5	180%

*Calculated as %increase in number of cells = $\frac{\text{number of cells at } t72 - \text{number of cells at } t0}{\text{number of cells at } t0} \times 100$



CHAPTER 4: CONCLUSION AND FUTURE PERSPECTIVES

4.1 Conclusion

The objectives of this study were to synthesize AuNPs from RW-Es, optimize the reaction parameters, characterize the AuNPs, and evaluate their potential wound healing activity. The AuNPs were successfully synthesized from three RW-Es, which served as both the reducing and stabilizing agents. A color change from yellow to a wine red indicated the presence of RW-AuNPs and was further confirmed by an SPR between 540 to 560nm, which is characteristic of AuNPs. When different reaction parameters such as temperature, pH, and concentrations were altered, the size and shape of the RW-AuNPs were tuned. Various functional groups responsible for the reduction of the gold salt to AuNPs were identified by FT-IR and suggested that the polyphenols, amino acids, and esters were most likely responsible for reducing the Au³⁺ and this was indicated as a chemical shift.

The antioxidant activities of the extracts and their respective AuNPs were evaluated through the DPPH assay. The RW-Es demonstrated a dose-dependent antioxidant and that of the AuNPs was satisfactory. The RW-AuNPs were stable in water, PBS, FBS, and DMEM for the test period as there were no significant changes observed in their UV-Vis spectra. The cell viability of KMST-6 cells treated with the RWEs and RW-AuNPs was not affected, indicating that the treatments were not cytotoxic. The PN-AuNPs reached an astounding 120% viability suggesting that these AuNPs accelerate the cell growth and wound closure following treatment with 50 µg/mL of RW-AuNPs for 72hrs. The results proved that the RW-AuNPs could be considered as growth enhancers and therefore be incorporated into wound healing ointments.

4.2 Recommendations

The main objectives of this mini-thesis study were successfully achieved however, more studies are needed to confirm the activity and specificity of these AuNPs. Further work to prove the wound-healing abilities of the RW-AuNPs, includes cell proliferation and migration studies in other cell lines (normal and diseased), and study their mechanism of action before considering an *in vivo* wound healing assay. The treatment time for wound healing were 72hrs however, stability tests were only done for 24hr, therefore stability in growth media as well as the shelf life should also be done for 72hrs. The RW-E

phytochemicals involved in the bio-reduction of RW-AuNPs will be identified and their role in the wound healing effect studied.



REFERENCES

- Abd El-Aziz, M., Badr, Y., & Mahmoud, M. A. (2007). Biosynthesis of gold nanoparticles using *Pseudomonas aeruginosa*. *AIP Conference Proceedings*, 888, 177–181. <https://doi.org/10.1063/1.2711108>
- Agyare, C., Boakye, Y. D., Bekoe, E. O., Hensel, A., Dapaah, S. O., & Appiah, T. (2016). Review: African medicinal plants with wound healing properties. *Journal of Ethnopharmacology*, 177, 85–100. <https://doi.org/10.1016/J.JEP.2015.11.008>
- Ahmad, T., Irfan, M., Bustam, M. A., & Bhattacharjee, S. (2016). Effect of Reaction Time on Green Synthesis of Gold Nanoparticles by Using Aqueous Extract of *Elaisa guineensis* (Oil Palm Leaves). *Procedia Engineering*, 148, 467–472. <https://doi.org/10.1016/J.PROENG.2016.06.465>
- Ahmed, S., Annu, Ikram, S., & Yudha, S. (2016). Biosynthesis of gold nanoparticles: A green approach. *Journal of Photochemistry and Photobiology B: Biology*, 161, 141–153. <https://doi.org/10.1016/J.JPHOTOBIO.2016.04.034>
- Ahmed, S., Ikram, S., & S, S. Y. (2016). Journal of Photochemistry & Photobiology , B : Biology Biosynthesis of gold nanoparticles : A green approach. *JPB*, 161, 141–153. <https://doi.org/10.1016/j.jphotobiol.2016.04.034>
- Ahmed, S., Ikram, S., & Salprima, Y. S. (2016). NU SC. *JPB*. <https://doi.org/10.1016/j.jphotobiol.2016.04.034>
- Ahn, E. Y., Lee, Y. J., Choi, S. Y., Im, A. R., Kim, Y. S., & Park, Y. (2018). Highly stable gold nanoparticles green-synthesized by upcycling cartilage waste extract from yellow-nose skate (*Dipturus chilensis*) and evaluation of its cytotoxicity, haemocompatibility and antioxidant activity. *Artificial Cells, Nanomedicine, and Biotechnology*, 46(sup2), 1108–1119. <https://doi.org/10.1080/21691401.2018.1479710>
- Akar, Z., Küçük, M., & Doğan, H. (2017). A new colorimetric DPPH • scavenging activity method with no need for a spectrophotometer applied on synthetic and natural antioxidants and medicinal herbs. *Journal of Enzyme Inhibition and Medicinal Chemistry*, 32(1), 640–647. <https://doi.org/10.1080/14756366.2017.1284068>
- Alberti, G., Zaroni, C., & Magnaghi, L. R. (2021). *Gold and Silver Nanoparticle-Based*

Colorimetric Sensors : New Trends and Applications.

- Ali, M. A., Ahmed, T., Wu, W., Hossain, A., Hafeez, R., Masum, M. M. I., Wang, Y., An, Q., Sun, G., & Li, B. (2020). Advancements in Plant and Microbe-Based Synthesis of Metallic Nanoparticles and Their Antimicrobial Activity against Plant Pathogens. *Nanomaterials*, 10(6), 1–24. <https://doi.org/10.3390/NANO10061146>
- Allen, S. L., Sharma, J. N., & Zamborini, F. P. (2017). Aggregation-Dependent Oxidation of Metal Nanoparticles. *Journal of the American Chemical Society*, 139(37), 12895–12898. https://doi.org/10.1021/JACS.7B05957/ASSET/IMAGES/LARGE/JA-2017-059579_0002.JPEG
- Amarnath, K., & Mathew, N. L. (2011). Facile synthesis of biocompatible gold nanoparticles from *Vitis vinefera* and its cellular internalization against HBL-100 cells. 121–132. <https://doi.org/10.1007/s12645-011-0022-8>
- Amarowicz, R. (2007). Tannins: The new natural antioxidants? *European Journal of Lipid Science and Technology*, 109(6), 549–551. <https://doi.org/10.1002/EJLT.200700145>
- Anastas, P., & Eghbali, N. (2010). Green Chemistry: Principles and Practice. *Chemical Society Reviews*, 39(1), 301–312. <https://doi.org/10.1039/b918763b>
- Arciero, J. C., Mi, Q., Branca, M., Hackam, D., & Swigon, D. (2013). Using a continuum model to predict closure time of gaps in intestinal epithelial cell layers. <https://doi.org/10.1111/j.1524-475X.2012.00865.x>
- Aziz Mousavi, S. M. A., Mirhosseini, S. A., Rastegar Shariat Panahi, M., & Mahmoodzadeh Hosseini, H. (2020). Characterization of Biosynthesized Silver Nanoparticles Using *Lactobacillus rhamnosus* GG and its In Vitro Assessment Against Colorectal Cancer Cells. *Probiotics and Antimicrobial Proteins*, 12(2), 740–746. <https://doi.org/10.1007/S12602-019-09530-Z>
- Bader, Y., Quint, R. M., & Getoff, N. (2008). Resveratrol products resulting by free radical attack. *Radiation Physics and Chemistry*, 77(6), 708–712. <https://doi.org/10.1016/j.radphyschem.2007.06.015>
- Baetke, S. C., Lammers, T., & Kiessling, F. (2015). Applications of nanoparticles for diagnosis and therapy of cancer. *The British Journal of Radiology*, 88(1054). <https://doi.org/10.1259/BJR.20150207>

- Balashanmugam, P., Balakumaran, M. D., Murugan, R., Dhanapal, K., & Kalaichelvan, P. T. (2016). Phyto-genic synthesis of silver nanoparticles , optimization and evaluation of in vitro antifungal activity against human and plant pathogens. *Microbiological Research*, 192, 52–64. <https://doi.org/10.1016/j.micres.2016.06.004>
- Barua, S., & Mitragotri, S. (2014). Challenges associated with Penetration of Nanoparticles across Cell and Tissue Barriers: A Review of Current Status and Future Prospects. *Nano Today*, 9(2), 223. <https://doi.org/10.1016/J.NANTOD.2014.04.008>
- Baruwati, B., & Varma, R. S. (2009). High value products from waste: grape pomace extract-a three-in-one package for the synthesis of metal nanoparticles. *ChemSusChem*, 2(11), 1041–1044. <https://doi.org/10.1002/CSSC.200900220>
- Beldon, P. (2010). Basic science of wound healing. *Surgery - Oxford International Edition*, 28(9), 409–412. <https://doi.org/10.1016/J.MPSUR.2010.05.007>
- Boomi, P., Ganesan, R., Prabu Poorani, G., Jegatheeswaran, S., Balakumar, C., Gurumallesh Prabu, H., Anand, K., Marimuthu Prabhu, N., Jeyakanthan, J., & Saravanan, M. (2020). Phyto-Engineered Gold Nanoparticles (AuNPs) with Potential Antibacterial, Antioxidant, and Wound Healing Activities Under in vitro and in vivo Conditions. *International Journal of Nanomedicine*, 15, 7553–7568. <https://doi.org/10.2147/IJN.S257499>
- Bors, W., Heller, W., Michel, C., & Saran, M. (1990). Flavonoids as antioxidants: determination of radical-scavenging efficiencies. *Methods in Enzymology*, 186(C), 343–355. [https://doi.org/10.1016/0076-6879\(90\)86128-I](https://doi.org/10.1016/0076-6879(90)86128-I)
- Bowler, P. G., Duerden, B. I., & Armstrong, D. G. (2001). Wound microbiology and associated approaches to wound management. *Clinical Microbiology Reviews*, 14(2), 244–269. <https://doi.org/10.1128/CMR.14.2.244-269.2001>
- Brause, R., Möltgen, H., & Kleinermanns, K. (2002). Characterization of laser-ablated and chemically reduced silver colloids in aqueous solution by UV/VIS spectroscopy and STM/SEM microscopy. *Applied Physics B: Lasers and Optics*, 75(6–7), 711–716. <https://doi.org/10.1007/s00340-002-1024-3>
- Caroline, S., & Barry, L. (2019). *Biogenic synthesis of gold nanoparticles using red and green pear fruit extracts. August.*

- Cedervall, T., Lynch, I., Foy, M., Berggård, T., Donnelly, S. C., Cagney, G., Linse, S., & Dawson, K. A. (2007). *Detailed Identification of Plasma Proteins Adsorbed on Copolymer*. 5754–5756. <https://doi.org/10.1002/anie.200700465>
- Chung, K. T., Wong, T. Y., Wei, C. I., Huang, Y. W., & Lin, Y. (1998). Tannins and human health: a review. *Critical Reviews in Food Science and Nutrition*, 38(6), 421–464. <https://doi.org/10.1080/10408699891274273>
- Coates, J. (2006). Interpretation of Infrared Spectra, A Practical Approach. *Encyclopedia of Analytical Chemistry*, 1–23. <https://doi.org/10.1002/9780470027318.a5606>
- Comino-Sanz, I. M., López-Franco, M. D., Castro, B., & Pancorbo-Hidalgo, P. L. (2021). The Role of Antioxidants on Wound Healing: A Review of the Current Evidence. *Journal of Clinical Medicine*, 10(16). <https://doi.org/10.3390/JCM10163558>
- Danaei, M., Dehghankhold, M., Ataei, S., Davarani, F. H., Javanmard, R., Dokhani, A., Khorasani, S., & Id, M. R. M. (2018). *Impact of Particle Size and Polydispersity Index on the Clinical Applications of Lipidic Nanocarrier Systems*. 1–17. <https://doi.org/10.3390/pharmaceutics10020057>
- Daruich, C., Souza, D., Nogueira, B. R., Elisa, M., & Rostelato, C. M. (2019). *Review of the methodologies used in the synthesis gold nanoparticles by chemical reduction*. <https://doi.org/10.1016/j.jallcom.2019.05.153>
- Dhivya, S., Padma, V. V., & Santhini, E. (2015). Wound dressings – a review. *BioMedicine*, 5(4), 24–28. <https://doi.org/10.7603/S40681-015-0022-9>
- Di Majo, D., La Guardia, M., Giammanco, S., La Neve, L., & Giammanco, M. (2008). The antioxidant capacity of red wine in relationship with its polyphenolic constituents. *Food Chemistry*, 111(1), 45–49. <https://doi.org/10.1016/J.FOODCHEM.2008.03.037>
- Domany, E. B. El, Essam, T. M., Ahmed, A. E., & Farghali, A. A. (2018). *Biosynthesis Physico-Chemical Optimization of Gold Nanoparticles as Anti- Biosynthesis Physico-Chemical Optimization of Gold Nanoparticles as Anti-Cancer and Synergetic Antimicrobial Activity Using Pleurotus ostreatus Fungus*. May. <https://doi.org/10.7324/JAPS.2018.8516>
- Dorosti, N., & Jamshidi, F. (2016). Plant-mediated gold nanoparticles by *Dracocephalum kotschyi* as anticholinesterase agent: Synthesis, characterization, and evaluation of

- anticancer and antibacterial activity. *Journal of Applied Biomedicine*, 14(3), 235–245.
<https://doi.org/10.1016/j.jab.2016.03.001>
- Dowsett, C. (2004). The use of silver-based dressings in wound care. *Nursing Standard (Royal College of Nursing (Great Britain) : 1987)*, 19(7), 56–60.
<https://doi.org/10.7748/ns2004.10.19.7.56.c3736>
- Dr. Levine, M. (2021). *ICP-OES – ICP Chemistry, ICP-OES Analysis, Strengths and Limitations / Technology Networks*.
<https://www.technologynetworks.com/analysis/articles/icp-oes-icp-chemistry-icp-oes-analysis-strengths-and-limitations-342265>
- Dreifke, M. B., Jayasuriya, A. A., & Jayasuriya, A. C. (2015). Current wound healing procedures and potential care. *Materials Science & Engineering. C, Materials for Biological Applications*, 48, 651. <https://doi.org/10.1016/J.MSEC.2014.12.068>
- Dube, P., Meyer, S., Madiehe, A., & Meyer, M. (2020). Antibacterial activity of biogenic silver and gold nanoparticles synthesized from *Salvia africana-lutea* and *Sutherlandia frutescens*. *Nanotechnology*, 31(50). <https://doi.org/10.1088/1361-6528/abb6a8>
- Dzimitrowicz, A., Jamroz, P., George, C., Gil, W., Motyka, A., Pogoda, D., & Pohl, P. (2017). Fermented juices as reducing and capping agents for the biosynthesis of size-defined spherical gold nanoparticles. *Journal of Saudi Chemical Society*.
<https://doi.org/10.1016/j.jscs.2017.12.008>
- Ealias, A. M., Saravanakumar, M. P., Ealias, A. M., & Saravanakumar, M. P. (2017). A review on the classification, characterisation, synthesis of nanoparticles and their application. *MS&E*, 263(3), 032019. <https://doi.org/10.1088/1757-899X/263/3/032019>
- Edelmann, A., Diewok, J., Schuster, K. C., & Lendl, B. (2001). *Rapid Method for the Discrimination of Red Wine Cultivars Based on Mid-Infrared Spectroscopy of Phenolic Wine Extracts*. 1139–1145.
- Elangkovan, D. R. A. J., & Ganapathy, D. (2020). *Benefits of Red Wine -A Review*. 26(2).
<https://doi.org/10.47750/cibg.2020.26.02.246>
- Elbagory, A. M., Cupido, C. N., Meyer, M., & Hussein, A. A. (2016). Large scale screening of southern African plant extracts for the green synthesis of gold nanoparticles using microtitre-plate method. *Molecules*, 21(11). <https://doi.org/10.3390/molecules21111498>

- Eming, S. A., Krieg, T., Davidson, J. M., & Hall, R. P. (2007). *Inflammation in Wound Repair : Molecular and Cellular Mechanisms*. 127(September 2006).
<https://doi.org/10.1038/sj.jid.5700701>
- Eskandari-nojehdehi, M., Jafarizadeh-malmiri, H., & Rahbar-shahrouzi, J. (2016).
Optimization of processing parameters in green synthesis of gold nanoparticles using microwave and edible mushroom (Agaricus bisporus) extract and evaluation of their antibacterial activity. <https://doi.org/10.1515/ntrev-2016-0064>
- Fernandez, K., & Agosin, E. (2007). Quantitative Analysis of Red Wine Tannins Using AND. *Journal of Agricultural and Food Chemistry*, 55(24), 7294–7300.
- Habib, A., Tabata, M., & Wu, Y. G. (2005). Formation of Gold Nanoparticles by Good's Buffers. [Http://Dx.Doi.Org/10.1246/Bcsj.78.262](http://Dx.Doi.Org/10.1246/Bcsj.78.262), 78(2), 262–269.
<https://doi.org/10.1246/BCSJ.78.262>
- Haiss, W., Thanh, N. T. K., Aveyard, J., & Fernig, D. G. (2007). *Determination of Size and Concentration of Gold Nanoparticles from UV - Vis Spectra*. 79(11), 4215–4221.
- Han, S. K. (2015). Innovations and advances in wound healing. *Innovations and Advances in Wound Healing*, 1–287. <https://doi.org/10.1007/978-3-662-46587-5>
- Harish, V., Tewari, D., Gaur, M., Yadav, A. B., Swaroop, S., Bechelany, M., & Barhoum, A. (2022). Review on Nanoparticles and Nanostructured Materials: Bioimaging, Biosensing, Drug Delivery, Tissue Engineering, Antimicrobial, and Agro-Food Applications. *Nanomaterials*, 12(3). <https://doi.org/10.3390/nano12030457>
- Hashmi, A. S. K., Blanco, M. C., Fischer, D., & Bats, J. W. (2006). Gold Catalysis: Evidence for the In-situ Reduction of Gold(III) During the Cyclization of Allenyl Carbinols. *European Journal of Organic Chemistry*, 2006(6), 1387–1389.
<https://doi.org/10.1002/EJOC.200600009>
- Hoag, G. E., Collins, J. B., Holcomb, J. L., Hoag, J. R., Nadagouda, M. N., & Varma, R. S. (2009). Degradation of bromothymol blue by 'greener' nano-scale zero-valent iron synthesized using tea polyphenols. *Journal of Materials Chemistry*, 19(45), 8671–8677.
<https://doi.org/10.1039/B909148C>
- Hsu, S. hui, Chang, Y. Bin, Tsai, C. L., Fu, K. Y., Wang, S. H., & Tseng, H. J. (2011). Characterization and biocompatibility of chitosan nanocomposites. *Colloids and*

Surfaces B: Biointerfaces, 85(2), 198–206.

<https://doi.org/10.1016/j.colsurfb.2011.02.029>

Iravani, S. (2011). Green synthesis of metal nanoparticles using plants. *Green Chemistry*, 13(10), 2638–2650. <https://doi.org/10.1039/C1GC15386B>

Jose, P., & Di, F. G. (2014). Aggregation behaviour of gold nanoparticles in saline aqueous media. <https://doi.org/10.1007/s11051-014-2376-4>

Khan, A. K., Rashid, R., Murtaza, G., & Zahra, A. (2014). Gold Nanoparticles: Synthesis and Applications in Drug Delivery. *Tropical Journal of Pharmaceutical Research*, 13(7), 1169–1177. <https://doi.org/10.4314/tjpr.v13i7.23>

Khan, I., Saeed, K., & Khan, I. (2019). Nanoparticles: Properties, applications and toxicities. In *Arabian Journal of Chemistry* (Vol. 12, Issue 7). <https://doi.org/10.1016/j.arabjc.2017.05.011>

Kim, M., Kim, J., Shin, Y. K., & Kim, K. Y. (2020). Gentisic Acid Stimulates Keratinocyte Proliferation through ERK1/2 Phosphorylation. *International Journal of Medical Sciences*, 17(5), 626. <https://doi.org/10.7150/IJMS.36484>

Korde, P., Ghotekar, S., Pagar, T., ... S. P.-J. of C., & 2020, U. (2020). Plant extract assisted eco-benevolent synthesis of selenium nanoparticles-a review on plant parts involved, characterization and their recent applications. *Jchemrev.Com*, 2(3), 157–168. https://www.researchgate.net/publication/340883196_Plant_Extract_Assisted_Eco-benevolent_Synthesis_of_Selenium_Nanoparticles-A_Review_on_Plant_Parts_Involved_Characterization_and_Their_Recent_Applications

Koushki, M., Amiri-Dashatan, N., Ahmadi, N., Abbaszadeh, H. A., & Rezaei-Tavirani, M. (2018). Resveratrol: A miraculous natural compound for diseases treatment. In *Food Science and Nutrition* (Vol. 6, Issue 8, pp. 2473–2490). Wiley-Blackwell. <https://doi.org/10.1002/fsn3.855>

Krishnaswamy, K., Vali, H., & Orsat, V. (2014). Value-adding to grape waste: Green synthesis of gold nanoparticles. *Journal of Food Engineering*, 142(June), 210–220. <https://doi.org/10.1016/j.jfoodeng.2014.06.014>

Lee, S. H., & Jun, B. H. (2019). Silver nanoparticles: Synthesis and application for nanomedicine. *International Journal of Molecular Sciences*, 20(4).

<https://doi.org/10.3390/ijms20040865>

- Li, C. J., & Chen, L. (2006). Organic chemistry in water. *Chemical Society Reviews*, 35(1), 68–82. <https://doi.org/10.1039/B507207G>
- Li, F., Fu, X., Huo, Q., & Chen, W. (2020). *Research progress on the nano-delivery systems of antitumor drugs*. <https://doi.org/10.1142/S1793984420400061>
- Li, J., Chen, J., & Kirsner, R. (2007). *Pathophysiology of acute wound healing*. 9–18. <https://doi.org/10.1016/j.clindermatol.2006.09.007>
- Li, N., Zhao, P., & Astruc, D. (2014). *Anisotropic Gold Nanoparticles : Synthesis , Properties , Applications , and Toxicity Angewandte*. 1756–1789. <https://doi.org/10.1002/anie.201300441>
- Li, X., Xu, H., Chen, Z., & Chen, G. (2011). *Biosynthesis of Nanoparticles by Microorganisms and Their Applications*. 2011. <https://doi.org/10.1155/2011/270974>
- Lundgaard, I., Wang, W., Eberhardt, A., Vinitzky, H. S., Reeves, B. C., Peng, S., Lou, N., Hussain, R., & Nedergaard, M. (2018). Beneficial effects of low alcohol exposure, but adverse effects of high alcohol intake on glymphatic function. *Scientific Reports*, 8(1), 1–16. <https://doi.org/10.1038/s41598-018-20424-y>
- Maggiolini, M., Recchia, A. G., Bonofiglio, D., Catalano, S., Vivacqua, A., Carpino, A., Rago, V., Rossi, R., & Andò, S. (2005). The red wine phenolics piceatannol and myricetin act as agonists for estrogen receptor in human breast cancer cells. *Journal of Molecular Endocrinology*, 35, 269–281. <https://doi.org/10.1677/jme.1.01783>
- Makarov, V., Sinitsyna, O. V, Yaminsky, I. V., & Taliansky, M. (2014). “ *Green* ” *Nanotechnologies : Synthesis of Metal Nanoparticles Using Plants*. March. <https://doi.org/10.32607/20758251-2014-6-1-35-44>
- Margolis, D. J., Hoffstad, O., Nafash, J., Leonard, C. E., Freeman, C. P., Hennessy, S., & Wiebe, D. J. (2011). Location, location, location: Geographic clustering of lower-extremity amputation among medicare beneficiaries with diabetes. *Diabetes Care*, 34(11), 2363–2367. <https://doi.org/10.2337/DC11-0807/-/DC1>
- Markoski, M. M., Garavaglia, J., Oliveira, A., Olivaes, J., & Marcadenti, A. (2016). Molecular properties of red wine compounds and cardiometabolic benefits. *Nutrition and Metabolic Insights*, 9, 51–57. <https://doi.org/10.4137/NMI.S32909>

- Masala, O., & Seshadri, R. (2004). SYNTHESIS ROUTES FOR LARGE VOLUMES OF NANOPARTICLES. *Http://Dx.Doi.Org/10.1146/Annurev.Matsci.34.052803.090949*, 34, 41–81. <https://doi.org/10.1146/ANNUREV.MATSCI.34.052803.090949>
- Meakin, P. (1984). *Diffusion-Limited Aggregation in Three Dimensions : Results from a New Cluster-Cluster Aggregation Model*. 102(2).
- Menon, S., S., R., & S., V. K. (2017). A review on biogenic synthesis of gold nanoparticles, characterization, and its applications. *Resource-Efficient Technologies*, 3(4), 516–527. <https://doi.org/10.1016/J.REFFIT.2017.08.002>
- MERCK. (2022). *Gold Nanoparticles: Properties and Applications*. <https://www.sigmaaldrich.com/ZA/en/technical-documents/technical-article/materials-science-and-engineering/biosensors-and-imaging/gold-nanoparticles>
- Mihai, mara madalina, Dima, M. B., Dima, B., & Holban, A. M. (2019). Nanomaterials in wound healing and infection control. *Materials*, 12(2176), 1–16. <https://doi.org/10.3390/ma12132176>
- Minasyan, H. (2019). Sepsis: mechanisms of bacterial injury to the patient. *Scandinavian Journal of Trauma, Resuscitation and Emergency Medicine* 2019 27:1, 27(1), 1–22. <https://doi.org/10.1186/S13049-019-0596-4>
- Moghaddam, A. B., Namvar, F., Moniri, M., Tahir, P. M., Azizi, S., & Mohamad, R. (2015). Nanoparticles Biosynthesized by Fungi and Yeast: A Review of Their Preparation, Properties, and Medical Applications. *Molecules (Basel, Switzerland)*, 20(9), 16540–16565. <https://doi.org/10.3390/MOLECULES200916540>
- Moodley, J. S., Babu, S., Krishna, N., Pillay, K., & Govender, P. (2020). Green Synthesis of Metal Nanoparticles for Antimicrobial Activity. *Novel Nanomaterials*. <https://doi.org/10.5772/INTECHOPEN.94348>
- Mordorski, B., Rosen, J., & Friedman, A. (2015). *Nanotechnology as an innovative approach for accelerating wound healing in diabetes*. 5, 329–332.
- Mosmann, T. (1983). *Rapid Colorimetric Assay for Cellular Growth and Survival : Application to Proliferation and Cytotoxicity Assays*. 65, 55–63.
- Murray, R. Z., West, Z. E., Cowin, A. J., & Farrugia, B. L. (2019). Development and use of biomaterials as wound healing therapies. *Burns & Trauma*, 7(1), 1–9.

<https://doi.org/10.1186/S41038-018-0139-7/FIGURES/6>

- Nadagouda, M. N., & Varma, R. S. (2008). Green synthesis of silver and palladium nanoparticles at room temperature using coffee and tea extract. *Green Chemistry*, 10(8), 859–862. <https://doi.org/10.1039/B804703K>
- Naskar, A., & Kim, K. (2020). *Recent Advances in Nanomaterial-Based Wound-Healing Therapeutics*.
- Ngungeni, Y. (n.d.). *Antimicrobial, anticancer and catalytic activities of green synthesized Avocado seed extract-gold nanoparticles*.
- Niska, K., Zielinska, E., Radomski, M. W., & Inkielewicz-stepniak, I. (2017). Metal nanoparticles in dermatology and cosmetology: Interactions with human skin cells. *Chemico-Biological Interactions*. <https://doi.org/10.1016/j.cbi.2017.06.018>
- Nqakala, Z. B., Sibuyi, N. R. S., Fadaka, A. O., Meyer, M., Onani, M. O., & Madiehe, A. M. (2021). Advances in nanotechnology towards development of silver nanoparticle-based wound-healing agents. In *International Journal of Molecular Sciences* (Vol. 22, Issue 20). <https://doi.org/10.3390/ijms222011272>
- Oh, J., & Chun, S. C. (2019). *Preparation and In Vitro Characterization of Chitosan Nanoparticles and Their Broad-Spectrum Antifungal Action Compared to Antibacterial Activities against Phytopathogens of Tomato*. <https://doi.org/10.3390/agronomy9010021>
- Oueslati, M. H., Tahar, L. Ben, & Harrath, A. H. (2020). Catalytic, antioxidant and anticancer activities of gold nanoparticles synthesized by kaempferol glucoside from Lotus leguminosae. *Arabian Journal of Chemistry*, 13(1), 3112–3122. <https://doi.org/10.1016/J.ARABJC.2018.09.003>
- Paladini, F., & Pollini, M. (2019). Antimicrobial silver nanoparticles for wound healing application: Progress and future trends. *Materials*, 12(16). <https://doi.org/10.3390/ma12162540>
- Pandey, K. B., & Rizvi, S. I. (2009). Plant polyphenols as dietary antioxidants in human health and disease. *Oxidative Medicine and Cellular Longevity*, 2(5), 270. <https://doi.org/10.4161/OXIM.2.5.9498>
- Pavliashvili, T., Kalabegishvili, T., Janjalia, M., Ginturi, E., & Tsertsvadze, G. (2017). *SYNTHESIS OF GOLD NANOPARTICLES FROM CHLOROAUIC ACID USING*

RED WINE. 192–195. <https://doi.org/10.17628/ecb.2017.6.192-195>

Peng, G., Tisch, U., Adams, O., Hakim, M., Shehada, N., Broza, Y. Y., Billan, S., Abdah-Bortnyak, R., Kuten, A., & Haick, H. (2009). Diagnosing lung cancer in exhaled breath using gold nanoparticles. *Nature Nanotechnology*, 4(10), 669–673.

<https://doi.org/10.1038/NNANO.2009.235>

Pentassuglia, S., Agostino, V., Tommasi, T., Torino, P., & Italiano, I. (2018). *EAB d Electroactive Biofilm : A Biotechnological Resource*. 110–123.

<https://doi.org/10.1016/B978-0-12-409547-2.13461-4>

Philip, D. (2008). *Synthesis and spectroscopic characterization of gold nanoparticles*. 71, 80–85. <https://doi.org/10.1016/j.saa.2007.11.012>

Pivodová, V., Franková, J., Galandáková, A., & Ulrichová, J. (2015). In Vitro AuNPs' Cytotoxicity and Their Effect on Wound Healing. *Nanobiomedicine*, 2, 1–7.

<https://doi.org/10.5772/61132>

Prathna, T. C., Chandrasekaran, N., Raichur, A. M., & Mukherjee, A. (2011). Colloids and Surfaces B : Biointerfaces Biomimetic synthesis of silver nanoparticles by Citrus limon (lemon) aqueous extract and theoretical prediction of particle size. *Colloids and Surfaces B: Biointerfaces*, 82(1), 152–159. <https://doi.org/10.1016/j.colsurfb.2010.08.036>

Rai, M., Ingle, A. P., Birla, S., Yadav, A., & Santos, C. A. Dos. (2016). Strategic role of selected noble metal nanoparticles in medicine. *Critical Reviews in Microbiology*, 42(5), 696–719. <https://doi.org/10.3109/1040841X.2015.1018131>

Rauh, A., Honold, T., & Karg, M. (2016). *Seeded precipitation polymerization for the synthesis of gold-hydrogel core-shell particles : the role of surface functionalization and seed concentration*. 37–47. <https://doi.org/10.1007/s00396-015-3782-6>

Raveendran, P., Fu, J., Wallen, S. L., Hill, C., & Carolina, N. (2003). *Completely “ Green ” Synthesis and Stabilization of Metal Nanoparticles*. 13940–13941.

Riaz, M., Zia-Ul-Haq, M., & Saad, B. (2016). *SPRINGER BRIEFS IN FOOD, HEALTH, AND NUTRITION Anthocyanins and Human Health: Biomolecular and therapeutic aspects*. Springer International Publishing. <https://doi.org/10.1007/978-3-319-26456-1>

Ribéreau-Gayon, P., Dubourdieu, D., Donèche, B., & Lonvaud, A. (2006). Handbook of Enology: Volume 1, The Microbiology of Wine and Vinifications. In *Handbook of*

Enology (Vol. 1). <https://www.cabdirect.org/cabdirect/abstract/20063192921>

Rónavári, A., Igaz, N., Adamecz, D. I., Szerencsés, B., Molnar, C., Kónya, Z., Pfeiffer, I., & Kiricsi, M. (2021). Green Silver and Gold Nanoparticles: Biological Synthesis Approaches and Potentials for Biomedical Applications. *Molecules* 2021, Vol. 26, Page 844, 26(4), 844. <https://doi.org/10.3390/MOLECULES26040844>

Saleh, H. E.-D. M., & Koller, M. (2018). Introductory Chapter: Principles of Green Chemistry. *Green Chemistry*. <https://doi.org/10.5772/INTECHOPEN.71191>

Salehi, B., Mishra, A. P., Nigam, M., Sener, B., Kilic, M., Sharifi-Rad, M., Fokou, P. V. T., Martins, N., & Sharifi-Rad, J. (2018). Resveratrol: A Double-Edged Sword in Health Benefits. *Biomedicines* 2018, Vol. 6, Page 91, 6(3), 91. <https://doi.org/10.3390/BIOMEDICINES6030091>

Sani, A., Cao, C., & Cui, D. (2021). Toxicity of gold nanoparticles (AuNPs): A review. *Biochemistry and Biophysics Reports*, 26, 100991. <https://doi.org/10.1016/j.bbrep.2021.100991>

Santhoshkumar, J., Rajeshkumar, S., & Venkat Kumar, S. (2017). Phyto-assisted synthesis, characterization and applications of gold nanoparticles – A review. *Biochemistry and Biophysics Reports*, 11, 46–57. <https://doi.org/10.1016/J.BBREP.2017.06.004>

Senapati, S., Mahanta, A. K., Kumar, S., & Maiti, P. (2018). Controlled drug delivery vehicles for cancer treatment and their performance. *Signal Transduction and Targeted Therapy*, 3(1). <https://doi.org/10.1038/S41392-017-0004-3>

Shah, M., Fawcett, D., Sharma, S., & Tripathy, S. K. (2015). *Green Synthesis of Metallic Nanoparticles via Biological Entities*. <https://doi.org/10.3390/ma8115377>

Shahverdi, S., Hajimiri, M., Amin, M., Akbar, A., & Dinarvand, R. (2014). Fabrication and structure analysis of poly (lactide-co-glycolic acid)/ silk fi broin hybrid scaffold for wound dressing applications. *Elsevier B.V.*, 473(1–2), 345–355. <https://doi.org/10.1016/j.ijpharm.2014.07.021>

Shahverdi, S., Hajimiri, M., Esfandiari, M. A., Larijani, B., Atyabi, F., Rajabiani, A., Dehpour, A. R., Gharehaghaji, A. A., & Dinarvand, R. (2014). Fabrication and structure analysis of poly(lactide-co-glycolic acid)/silk fibroin hybrid scaffold for wound dressing applications. *International Journal of Pharmaceutics*, 473(1–2), 345–355.

<https://doi.org/10.1016/j.ijpharm.2014.07.021>

Shamsaie, A., Jonczyk, M., Sturgis, J., Paul Robinson, J., & Irudayaraj, J. (2007).

Intracellularly grown gold nanoparticles as potential surface-enhanced Raman scattering probes. *Journal of Biomedical Optics*, 12(2), 020502. <https://doi.org/10.1117/1.2717549>

Shankar, S., Braja, D., & Bag, G. (2014). *Synthesis of gold nanoparticles using renewable Punica granatum juice and study of its catalytic activity*. 55–59.

<https://doi.org/10.1007/s13204-012-0179-4>

Shanmugasundaram, T., Radhakrishnan, M., Gopikrishnan, V., Kadirvelu, K., &

Balagurunathan, R. (2017). *RSC Advances In vitro antimicrobial and in vivo wound healing effect of actinobacterially synthesised nanoparticles of silver , gold and their alloy* †. 51729–51743. <https://doi.org/10.1039/c7ra08483h>

Sherwani, M. A., Tufail, S., Khan, A. A., & Owais, M. (2015). *Gold Nanoparticle-Photosensitizer Conjugate Based Photodynamic Inactivation of Biofilm Producing Cells : Potential for Treatment of C . albicans Infection in BALB / c Mice*. 1–20.

<https://doi.org/10.1371/journal.pone.0131684>

Shi, W., Casas, J., Venkataramasubramani, M., & Tang, L. (2012). *Synthesis and Characterization of Gold Nanoparticles with Plasmon Absorbance Wavelength Tunable from Visible to Near Infrared Region*. 2012. <https://doi.org/10.5402/2012/659043>

Sibuyi, Nicole Remaliah S, Thovhogi, N., Gabuza, K. B., Meyer, M. D., Drah, M., Onani, M. O., Skepu, A., Madiehe, A. M., & Meyer, M. (2017). Peptide-functionalized nanoparticles for the selective induction of apoptosis in target cells. *Nanomedicine*, 12(14), 1631–1645. <https://doi.org/10.2217/nnm-2017-0085>

Sibuyi, Nicole Remaliah Samantha, Thipe, V. C., Panjtan-Amiri, K., Meyer, M., & Katti, K. V. (2021). Green synthesis of gold nanoparticles using Acai berry and Elderberry extracts and investigation of their effect on prostate and pancreatic cancer cells. *Nanobiomedicine*, 8, 184954352199531. <https://doi.org/10.1177/1849543521995310>

Singh, S., Young, A., & McNaught, C. E. (2017). The physiology of wound healing. *Surgery (Oxford)*, 35(9), 473–477. <https://doi.org/10.1016/J.MPSUR.2017.06.004>

Singhal, D., & Saxena, S. (2015). Screening and Toxicity Analysis of Catechin Isomers Against FemA Protein. *Indian Journal of Pharmaceutical Sciences*, 77(6), 758–763.

<https://doi.org/10.4103/0250-474X.174968>

Slepička, P., Kasálková, N. S., Siegel, J., Kolská, Z., & Švorčík, V. (2020). Methods of Gold and Silver Nanoparticles Preparation. *Materials*, *13*(1), 1.

<https://doi.org/10.3390/MA13010001>

Snopek, L., Mlcek, J., Sochorova, L., Baron, M., Hlavacova, I., Jurikova, T., Kizek, R., Sedlackova, E., & Sochor, J. (2018). Contribution of red wine consumption to human health protection. *Molecules*, *23*(7), 1–16. <https://doi.org/10.3390/molecules23071684>

Sokolsky-Papkov, M., & Kabanov, A. (2019). Synthesis of well-defined gold nanoparticles using Pluronic: The role of radicals and surfactants in nanoparticles formation.

Polymers, *11*(10). <https://doi.org/10.3390/polym11101553>

Sousa, L. M., Vilarinho, L. M., Ribeiro, G. H., Bogado, A. L., & Dinelli, L. R. (2017). An electronic device based on gold nanoparticles and tetra-ruthenated porphyrin as an electrochemical sensor for catechol. *Royal Society Open Science*, *4*(12).

<https://doi.org/10.1098/RSOS.170675>

Stozhko, N. Y., Bukharinova, M. A., Khamzina, E. I., Tarasov, A. V., Vidrevich, M. B., & Brainina, K. Z. (2019). The Effect of the Antioxidant Activity of Plant Extracts on the Properties of Gold Nanoparticles. *Nanomaterials*, *9*(12).

<https://doi.org/10.3390/NANO9121655>

Stratil, P., Kubáň, V., & Fojtová, J. (n.d.). Comparison of the Phenolic Content and Total Antioxidant Activity in Wines as Determined by Spectrophotometric Methods. *Czech J. Food Sci*, *26*(4), 242–253.

Strober, W. (2001). Trypan blue exclusion test of cell viability. *Current Protocols in Immunology*, Appendix 3. <https://doi.org/10.1002/0471142735.IMA03BS21>

Stuchinskaya, T., Moreno, M., Cook, M. J., Edwards, D. R., & Russell, D. A. (2011). Targeted photodynamic therapy of breast cancer cells using antibody-phthalocyanine-gold nanoparticle conjugates. *Photochemical & Photobiological Sciences : Official Journal of the European Photochemistry Association and the European Society for Photobiology*, *10*(5), 822–831. <https://doi.org/10.1039/C1PP05014A>

Styger, G., Prior, B., & Bauer, F. F. (2011). *Wine flavor and aroma*. 1145–1159.

<https://doi.org/10.1007/s10295-011-1018-4>

- Thompson, D. T. (2007). Using gold nanoparticles for catalysis. *Nano Today*, 2(4), 40–43. [https://doi.org/10.1016/S1748-0132\(07\)70116-0](https://doi.org/10.1016/S1748-0132(07)70116-0)
- Tsekhmistrenko, S. I., Bityutskyy, V. S., Tsekhmistrenko, O. S., Horalskyi, L. P., Tymoshok, N. O., & Spivak, M. Y. (2020). Bacterial synthesis of nanoparticles: A green approach. In *Biosystems Diversity* (Vol. 28, Issue 1, pp. 9–17). Oles Honchar Dnipro National University. <https://doi.org/10.15421/012002>
- Tyavambiza, C., Dube, P., Goboza, M., Meyer, S., Madiehe, A. M., & Meyer, M. (2021). *Medicinal Plants and Their Synthesized Biogenic Nanoparticles*. 1–14.
- Veeraputhiran, V. (2013). *Bio-Catalytic Synthesis of Silver Nanoparticles*. 5(5), 2555–2562.
- Vijayakumar, S., Vaseeharan, B., Malaikozhundan, B., Gopi, N., Ekambaram, P., Pachaiappan, R., Velusamy, P., Murugan, K., Benelli, G., Suresh Kumar, R., & Suriyanarayanamoorthy, M. (2017). Therapeutic effects of gold nanoparticles synthesized using *Musa paradisiaca* peel extract against multiple antibiotic resistant *Enterococcus faecalis* biofilms and human lung cancer cells (A549). *Microbial Pathogenesis*, 102, 173–183. <https://doi.org/10.1016/J.MICPATH.2016.11.029>
- Wang, L., & Stoner, G. D. (2008). *Anthocyanins and their role in cancer prevention*. 269, 281–290. <https://doi.org/10.1016/j.canlet.2008.05.020>
- Wang, S., & Lu, G. (2018). Applications of Gold Nanoparticles in Cancer Imaging and Treatment. In *Noble and Precious Metals - Properties, Nanoscale Effects and Applications*. <https://doi.org/10.5772/intechopen.70901>
- Wang, Y. C., & Gunasekaran, S. (2012). Spectroscopic and microscopic investigation of gold nanoparticle nucleation and growth mechanisms using gelatin as a stabilizer. *Journal of Nanoparticle Research*, 14(10). <https://doi.org/10.1007/s11051-012-1200-2>
- Wang, Y., & Xia, Y. (2004). Bottom-up and top-down approaches to the synthesis of monodispersed spherical colloids of low melting-point metals. *Nano Letters*, 4(10), 2047–2050. <https://doi.org/10.1021/nl048689j>
- Zhang, W. (2014). Nanoparticle aggregation: principles and modeling. *Advances in Experimental Medicine and Biology*, 811, 20–43. https://doi.org/10.1007/978-94-017-8739-0_2
- Zhao, J., & Friedrich, B. (2015). Synthesis of gold nanoparticles via chemical reduction

methods. *NANOCON 2015 - 7th International Conference on Nanomaterials - Research and Application, Conference Proceedings*, 597–604.

Zheng, L. T., Ryu, G. M., Kwon, B. M., Lee, W. H., & Suk, K. (2008). Anti-inflammatory effects of catechols in lipopolysaccharide-stimulated microglia cells: inhibition of microglial neurotoxicity. *European Journal of Pharmacology*, 588(1), 106–113.
<https://doi.org/10.1016/J.EJP HAR.2008.04.035>

